2013

Optimal grasping of soft objects with two robotic fingers

Huan Lin
Iowa State University

Optimal grasping of soft objects with two robotic fingers

by

Huan Lin

A thesis submitted to the graduate faculty

in partial fulfillment of the requirements for the degree of

MASTER OF SCIENCE

Major: Computer Science

Program of Study Committee:

Yan-Bin Jia, Major Professor

Guang Song

James Oliver

Iowa State University

Ames, Iowa

2013

DEDICATION

I would like to dedicate this thesis to my family without whose support I would not have been able to complete this work. I would also like to thank my friends for their loving guidance and during the writing of this work.

TABLE OF CONTENTS

LIST OF TABLES

LIST OF FIGURES

ACKNOWLEDGEMENTS

I would like to take this opportunity to express my thanks to those who helped me with various aspects of conducting research and the writing of this thesis. First and foremost, Dr. Yanbin Jia for his guidance, patience and support throughout this research and the writing of this thesis. His insights and words of encouragement have often inspired me and renewed my hopes for completing my graduate education. I would also like to thank my committee members for their efforts and contributions to this work: Dr. Guang Song and Dr. James Oliver.

ABSTRACT

Robot grasping of deformable objects is an under-researched area. The difficulty comes from both mechanics and computation. First, deformation caused by the grasp operations changes object's global geometry. Second, under deformation, an object's contacts with the fingers grow from points into areas. Inside such a contact area, points that stick to the finger may later slide while points that slide may later stick. The torques exerted by the grasping fingers vary, in contrast with rigid body grasping whose torques are invariant under forces.

In this thesis the object's deformation and configuration of contact with fingers and the plane are tracked with finite element method(FEM) in an event-driven manner based on the contact displacements induced by the finger movements.

The first part of this thesis analyzes two-finger squeeze grasping of deformable objects with a focus on two special classes: *stable squeezes*, which minimize the potential energy of the object among squeezes of the same depth, and *pure squeezes*, which eliminate all euclidean motions from the resulting deformations. Based on them an algorithm to characterize the best resistance by a grasp to an adversary figner is proposed which minimizes the work done by the grasping fingers. An optimization scheme is offered to handle the general case of frictional segment contact. Simulations and multiple experiments with a Barrett Hand on a rubber foam object are presented.

The second part of this thesis describes a strategy for a two-finger robot hand to grasp and lift a 3D deformable object resting on the plane. Inspired by the human hand grasping, the strategy employs two rounded fingers to squeeze the object until a secure grasp is achieved under contact friction. And then lift it by translating upward to pick

up the object. During the squeeze, a lift test is repeatedly conducted until it is successful based on the metrics and then trigger the upward translation. The gravitational force acting on the object is accounted for. Simulation is presented and shows some good promise for the sensorless grasping approach for deformable objects.

CHAPTER 1. INTRODUCTION

The difficulty of robot grasping of deformable objects comes from both mechanics and computation. First of all, deformation caused by the grasp actions changes the global geometry of the object. Second, during deformation an object's contacts with the fingers grow from points into areas. Inside the contact area, points that stick to the finger may later slide while points that slide may later stick. The torques exerted by the grasping fingers vary, in contrast with rigid body grasping whose torques are invariant under forces.

Determining a small deformation based on linear elasticity ends up with down to solving a system of fourth order differential equations (1), which has no closed-form solution generally. In practice, effiecient computation is conducted using finite element method (FEM) (2) which relies on positional constraints. That is because the stiffness matrix of an unconstrained object has a null space consists of all its rigid body motions. All of the above implies that the displacements of some points of the object need to be specify to carry on deformable modeling during a grasp.

In this thesis we choose to specify the desired displacements of the grasping fingers and the points on the plane instead of the force they exert. In practice it is much easier to command a finger to move to a specific position than to control it to exert a designated force. Also, forces are not much of our concern here as long as the object can be grasped in our task.

In the first part of the thesis , we investigate how to characterize the quality of a squeeze grasp in 2D grasping proposed in (3). A successfull rigid body grasp must

not induce any movement of the contact points. Existing metrics for the quality for rigid body grasping are force-centered, either to maximize the worst-case adversary force resistance by a unit total grasping force (6), (8), to minimize the maximum finger contact force to resist the adversary force (9), (10), or to minimize the possibility of violating some hard constraints (4), (5). We refer to (11) for a comprehensive summary on various rigid body grasp metrics.

Howerver, on deformable objects, the grasping fingers perform some work due to deformation, most of which is converted to strain energy. Therefore it makes sense to have an energy-based metric for measuring the quality of grasp. The deformation-space approach (13) was proposed byGopalakrishnan and Goldberg to characterize the optimal grasp as the one from which the potential energy needed for a release is equal to the amount at the elastic limit of the object. In this thesis, we present the measure by the amount of the work performed by the grasping fingers to resist a distrurbing finger under known displacement.

The second part of the thesis introduces a simple strategy for a robot hand without using tactile sensing to pick up 3D deformable objects at rest. Human hands are experienced at handling deformable objects in daily life. To pick up a soft object sitting on the table, for instance, human hand usually squeezes it using two or more fingers to achieve a firm grasp, leveraing the table's support to ensure stability. After that the hand, considering the object's mass and contact friction, starts to lift it up at some point. During the lift as an increasing portion of the obejct's weight is felt, the hand may apply extra squeeze to prevent slips. Inspired by human hand grasping, our strategy for robot hands is to squeeze an object and shortly, after every extra amount of squeeze, they perform a lift test to check if the obejct is able to be lifted. Once the test is passed, the fingers stop squeezing and pick up the object via upward translation. Through out the process, the object is fully constrained by the fingers, with or without the supporting plane.

1.1 Assumptions

In this thesis we assume that the entire operation causes by small deformatios of the object that can be describe wtihin the scope of linear elasticity. In the classical elasticity theory, deformation happens instantaneously. Here we will sometimes consider deformation as a continuous process which happens in an infinitesimal amount of time, in order to capture the varying contact area between the object and the fingers and changing contact modes of contact nodes.

The initial finger placement needs to prevent all Euclidean motions. In the presence of friction, the placement needs to be force closure if the object were rigid. From the result by (14), the segment connecting the two initial contact points must lie inside their friction cones. Under a squeeze, each contact point will grow into a segment in which the points may switch their contact modes between stick and slip. The contact segment is not regarded as sliding as long asat least one point on the segment sticks.

For 2D grasping, we make the following assumptions:

1. The object is isotropic, and either plannar or thin 2-$\frac{1}{2}$D.

2. Gravity is ignored.

3. The fingers are rigid and coplanar with the object and make frictional contact with it.

And also the fingers are with semicircular tips in 2D grasping and with semispherical tips in 3D case.

The thesis uses meter for length, Pascal for pressure, Newton for force, and Joule for work and energy. The units are omitted from now on.

1.2 Organization of the Thesis

The rest of the manuscript is organized as follows.

Chapter 2 surveys related work in robot grasping on rigid body and deformable objects.

Chapter 3 will briefly review some basics of linear elasticity, fourndation of squeezing , and characterize stable and pure squeezes of a deformable object.

In Chapter 4, we will construct grasps that perform minimum work to resist an adversary finger, progressing from the cases of fixed point and segment contacts to that of frictional segment contacts.

In Chapter 5, we propose a simple strategy for a robot hand to grasp and lift a deformable 3D object resting on a table.

Chapter 6 discusses the future work.

CHAPTER 2. RELATED WORK

Rigid body grasping is an extensively studied area rich with theoretical analyses, algorithmic syntheses, simulations and experiments with robotic hands (15). First-order form closure (16) is widely regarded as equivalent to force closure with frictionless contacts. Mishra (12) gave upper bounds on the numbers of contact points sufficient and/or necessary for form closure. Tighter bounds were later derived for 2D and 3D objects with piecewise smooth boundaries (7). Algorithms were proposed to compute all form closure grasps of polygonal parts (17; 18). There was also some work (19; 20) on caging an object with imposed frictionless contacts so that it could move inside but not escape.

Two-finger force-closure grasps of 2D objects are efficiently computable for both polygons (14) and piecewise smooth curved shapes (22). Ponce (21) also developed algorithms for grasping 3D objects. Trinkle (23) formulated the force-closure test as a linear program with an objective function which characterized the quality as the distance from losing the closure.

The introduction of task ellipsoid (5) formalized the idea that the choice of a grasp should be based on the capacity to generate wrenches that were relevant to the task. Grasp quality measures for multifingered hands were proposed to consider selection of internal grasping forces that were furthest from violating any closure, friction, or mechanical constraints (4), or were directly derived from the grasp matrix which characterized the wrench space of a grasp (5). Grasp metrics for polygons and polyhedra often sought to maximize the worst-case external force that could be resisted by a unit grasping force (6; 8; 24). A summary was given by Mishra (11) on various grasp metrics, addressing

the trade-offs among grasp goodness, object geometry, the number of fingers, and the computational complexity for grasp synthesis. Some recent work (10; 9) applied semidefinite programming techniques to minimize the maximum magnitude of the contact force at any frictional contact of a grasp in order to maintain equilibrium against a known adversary wrench .

There was not much work when it comes to grasping deformable objects, a difficult problem that needs to deal with changing local contact geometry as well as the global object geometry caused by the physical deformation. The notion of bounded force-closure (27) was introduced for this type of grasps. Hirai (28) controlled the motion of a grasped deformable effectively object with visual and tactile information. The deformation-space approach (13) characterized the optimal grasp of a deformable part as the one from which the potential energy needed for a release equals the amount at the parts elastic limit.

In contrast, manipulation of flexible linear objects such as wires or ropes has been a very active area, with work on static modeling (26), knotting and unknotting (29; 30; 31; 25), pickup (32), and path planning (33). These operations, however, can be carried out without a need for deformable modeling.

Sinha and Abel (34) proposed a model for deformation of the contact regions under a grasp, predicting normal and tangential contact forces with no concern of global deformation or grasp computation. Luo and Xiao (35) demonstrated that simulation accuracy and efficiency could be improved based on derived geometric properties at a deformable contact. Tian and Jia (36) investigated deformable modeling of shell-like objects that were already grasped under point contacts.

More thorough investigations on the elastic contact problem were conducted by the mechanics community regarding the contact area between two deformable bodies under a known applied load. The gradual nature of the physical process suggests iterative updates of the growing contact region(s). In the work by Francavilla and Zienkiewicz (37), an FEM-based solution was given for 2D elastic contact problems under frictionless

contacts. It was extended to incorporate Coulomb friction by Okamoto and Nakazawa (38) and Sachdeva and Ramakrishnan (39) via iterative updating of the contact area and the modes of individual contact nodes: stick, slip, contact establishment, or contact break. In each iteration, FEM computed the deformed shape based on position and friction constraints derived from the contact modes under Coulomb friction. This event-based approach was extended by Chandrasekaran et al. (40) to handle geometric and physical nonlinearities as well as node-edge contacts in solving for the exact loading condition from prescribed displacements.

Guo(3) investigated squeeze grasping of deformable 2D objects. One of the ideas reflecting a key difference from rigid body grasping, was to specify the finger movements rather than finger forces. This is because force and torque equilibrium are guaranteed over a deforming body which is fully constrained, following (1), (41). Another idea was to obtain the constraints needed for deformation updates from the contact sets with the fingers, which are modified in an event-driven manner during the deformation.

CHAPTER 3. STABLE AND PURE SQUEEZES

This chapter begins with a review of plane linear elasticity, and then introduces the notions of pure and stable squeezes of an object induced by the specified movements of a subset of boundary points.

3.1 Linear Plane Elasticity

Consider a thin flat object shown in Figure 3.1 with thickness h significantly less than its two other dimensions. Essentially, the object is a generalized cylinder which results from translating the region S bounded by a closed simple curve in the xy-plane along the z-direction upward and downward each by $h/2$. The origin is placed at the centroid of S.

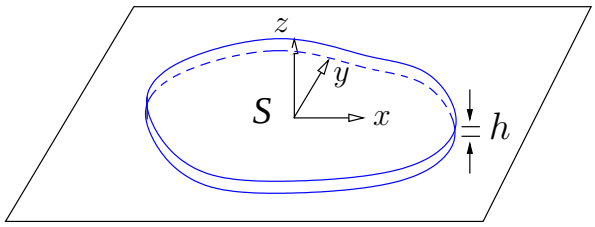

Figure 3.1 Thin flat object.

In this part, we consider *plane stress* (42) parallel to the xy-plane which means zero normal stress along the z-axis and zero shear stresses in the x-z and y-z planes. Under a *displacement field* $\boldsymbol{\delta} = (u(x,y), v(x,y))^T$, every point $(x,y)^T$ inside S moves to $(x+u, y+v)^T$. The same displacement applies to the points of the object that are

vertically above or below the point $(x, y)^T$. The normal strains ϵ_x and ϵ_y along the x- and y-axes, respectively, and the shearing strain γ_{xy} are given below:

$$\begin{aligned} \epsilon_x &= \frac{\partial u}{\partial x}, \\ \epsilon_y &= \frac{\partial v}{\partial y}, \\ \gamma_{xy} &= \frac{\partial u}{\partial y} + \frac{\partial v}{\partial x}. \end{aligned} \tag{3.1}$$

Under Hooke's law, the following stress-strain relationships hold:

$$\begin{aligned} \epsilon_x &= \frac{\sigma_x - \nu\sigma_y}{E}, \\ \epsilon_y &= \frac{\sigma_y - \nu\sigma_x}{E}, \\ \gamma_{xy} &= \frac{\tau_{xy}}{G} = \frac{2(1+\nu)}{E}\tau_{xy}, \end{aligned} \tag{3.2}$$

where E and ν are Young's modulus and Poisson's ratio of the material, respectively, σ_x and σ_y are the normal stress components in the x- and y-directions, respectively, and τ_{xy} is the shear stress in the x-y plane. The strain energy of the object (1) is

$$U = \frac{h}{2}\iint_S \left(\frac{E}{1-\nu^2}(\epsilon_x^2 + 2\nu\epsilon_x\epsilon_y + \epsilon_y^2) + \frac{E}{2(1+\nu)}\gamma_{xy}\right)dxdy. \tag{3.3}$$

Suppose $\boldsymbol{\delta}$ is the displacment vector caused by external forces applied in the plane at some boundary points, which forms a set Γ. Denote by $\boldsymbol{f}(x, y)$ the force exerts at point $(x, y)^T \in \Gamma$. The total potential of the applied forces is

$$W = -\sum_{(x,y)^T \in \Gamma} \boldsymbol{\delta}(x, y)^T \boldsymbol{f}(x, y). \tag{3.4}$$

The total potential energy of the system is

$$\Pi = U + W. \tag{3.5}$$

The principle of minimum potential energy states that $\boldsymbol{\delta}$ minimizes Π.

3.2 Foundation of Squeezing

This section goes through a quick review of (3) on squeeze grasp with two fingers in 2D grasping. The cross section of the object is discretized into small uniform triangular elements with n vertices. Minimization of the potential energy yields the familiar constitutive equation: $K\boldsymbol{\delta} = \boldsymbol{f}$, where K is the shape's stiffness matrix that is symmetric and positive semi-definite with rank $2n-3$, $\boldsymbol{\delta}$ is the displacement vector, and $\boldsymbol{f}$ is the external force vector.

The matrix assumes a spectral decomposition that

$$K = V\Lambda V^T, \tag{3.6}$$

where $V = (v_{ij}) = (\boldsymbol{v}_1, \boldsymbol{v}_2, ..., \boldsymbol{v}_{2n})$ and $\Lambda = diag(\lambda_1, ..., \lambda_{2n-3}, 0, 0, 0)$. The null space of K is spanned by the following three vectors which represent translations and pure rotation:

$$\boldsymbol{v}_{2n-2} = \frac{(1,0,...,1,0)^T}{\sqrt{n}}, \boldsymbol{v}_{2n-1} = \frac{(0,1,...,0,1)^T}{\sqrt{n}}, \text{and } \boldsymbol{v}_{2n} = \frac{\boldsymbol{r}}{\|\boldsymbol{r}\|}, \tag{3.7}$$

where $\boldsymbol{r}$ is the component of $(-y_1, x_1, ..., -y_n, x_n)^T$ that is orthogonal to $\boldsymbol{v}_{2n-2}$ and $\boldsymbol{v}_{2n-1}$.

The grasp strategy is to specify the displacements $\boldsymbol{\delta}_t$ of m boundary contact nodes $\boldsymbol{p}_t$, $t \in \mathbb{I}$. Denote by $\bar{\boldsymbol{v}}_l$, $1 \le l \le 2m$, the $2m$-vector that aggregates $v_{2t-1,l}$ and $v_{2t,l}$, for all $t \in \mathbb{I}$, in the increasing index order. Introduce the matrix

$$M = \begin{pmatrix} A & B \\ B^T & \mathbf{0} \end{pmatrix}, \tag{3.8}$$

where $A = \sum_{l-1}^{2n-3} \frac{1}{\lambda_l} \bar{\boldsymbol{v}}_l \bar{\boldsymbol{v}}_l^T$ and $B = (\bar{\boldsymbol{v}}_{2n-2}, \bar{\boldsymbol{v}}_{2n-1}, \bar{\boldsymbol{v}}_{2n})$. It was shown in (3) that the $(2m+3) \times (2m+3)$ matrix M has an inverse when $m \ge 2$:

$$M^{-1} = \begin{pmatrix} C & E \\ E^T & -E^T A E \end{pmatrix}, \tag{3.9}$$

where C is symmetric and of dimenstion $2m \times 2m$.

Deformation is uniquely determined for $m \geq 2$ under specified $\boldsymbol{\delta}_t$, $t \in \mathbb{I}$, and $\boldsymbol{f}_l = 0$, $l \notin \mathbb{I}$. Apply the same bar notation to select entries with indices $i \in \mathbb{I}$ from the force vector $\boldsymbol{f}$ and the displacement field $\boldsymbol{\delta}$. We have

$$\bar{\boldsymbol{f}} = C\bar{\boldsymbol{\delta}} \quad \text{and} \quad \boldsymbol{\delta} = H\bar{\boldsymbol{\delta}}, \tag{3.10}$$

for some $2n \times 2m$ matrix H. The submatrix C is referred to as the *reduced stiffness matrix*. The strain energy of the object is

$$U = \frac{1}{2}\bar{\boldsymbol{\delta}}^T C\bar{\boldsymbol{\delta}}. \tag{3.11}$$

3.3 Stable Squeezes

Denoted by $\mathcal{G}(\boldsymbol{p}_i, \boldsymbol{p}_j)$ the placement of two fingers $\mathcal{F}_1$ and $\mathcal{F}_2$ at the nodes $\boldsymbol{p}_i$ and $\boldsymbol{p}_j$. For clarity of description, in this section we assume that $\mathcal{F}_1$ and $\mathcal{F}_2$ are point fingers, and $\boldsymbol{p}_i$ and $\boldsymbol{p}_j$ will always stay as the only contact points during a grasp operation by the fingers as if it is glued with the object.

Theorem 3.3.1. *Suppose $m \geq 2$. The following statements hold for the submatrices of M and M^{-1}.*

(1) rank(B) = 3.

(2) C is symmetric and positive semi-definite such that null(C) = col(B). This implies that the 2m-dimensional space is a direct sum of the column spaces of C and B:

$$\mathbb{R}^{2m} = col(C) \oplus col(B). \tag{3.12}$$

(3) rank(AC) = 2m − 3 and AC has only one eigenvalue 1 (of multiplicity 2m − 3).

(4) $\mathbb{R}^{2m} = col(AC) \oplus col(E)$.

For stability reason we want to determine the direction under the same amount of squeeze that minimizes the potential energy

$$\Pi = U - \boldsymbol{\delta}^T\boldsymbol{f} = U - \bar{\boldsymbol{\delta}}^T\bar{\boldsymbol{f}} = -\frac{1}{2}\bar{\boldsymbol{\delta}}^T C\bar{\boldsymbol{\delta}}. \tag{3.13}$$

by equations 3.10 and 3.11. Because $m = 2$, $\text{rank}(C) = 4 - \text{rank}(B) = 1$ following Theorem 3.3.1. It is clear that Π is minimized by a unit vector orthogonal to col(B). We can easily show that

$$\hat{\boldsymbol{u}} = \frac{1}{\sqrt{2}\|\boldsymbol{p}_i - \boldsymbol{p}_j\|} \begin{pmatrix} \boldsymbol{p}_j - \boldsymbol{p}_i \\ \boldsymbol{p}_i - \boldsymbol{p}_j \end{pmatrix} \tag{3.14}$$

is such a unit vector. Indeed, it is the only one corresponding to a grasp because $-\hat{u}$ pulls at the contacts.

Theorem 3.3.2. *$\hat{\boldsymbol{u}}$ is orthogonal to null(C). Moreover,*

$$C = \frac{1}{\hat{\boldsymbol{u}}^T A \hat{\boldsymbol{u}}} \hat{\boldsymbol{u}} \hat{\boldsymbol{u}}^T. \tag{3.15}$$

We refer to a movement of $\mathcal{F}_1$ and $\mathcal{F}_2$ specified by $\bar{\boldsymbol{\delta}} = \rho \hat{\boldsymbol{u}}, \rho > 0$, as a *stable squeeze*, so called because it minimizes the systems potential energy among all squeezes of magnitude ρ. Substituting $\hat{\boldsymbol{\delta}} = \rho \hat{\boldsymbol{u}}$ and equation 3.3.2 into 3.11, we obtain the strain energy

$$U_s = \rho^2 / (2 \hat{\boldsymbol{u}}^T A \hat{\boldsymbol{u}}). \tag{3.16}$$

3.4 Pure Squeezes

A stable squeeze is good since it minimize the potential energy. However, it does not guarantee that the resulting displacement field has no rigid body motion component. Since linear elasticity cannot describe large rotation, sometimes we would like to avoid rotation. That is why we introduce pure squeeze which yields no rigid body motion. This is equivalent to $E^T \bar{\boldsymbol{\delta}} = 0$ as we can establish using equation 3.10. By Theorem 3.3.1, the set col(AC) includes all pure squeezes. Since $AC = A\hat{\boldsymbol{u}}\hat{\boldsymbol{u}}^T / (\hat{\boldsymbol{u}}^T A \hat{\boldsymbol{u}})$ following Theorem 3.3.2, we can infer that col(AC) is spanned by $A\hat{\boldsymbol{u}}$. Let $\hat{\boldsymbol{v}} = A\hat{\boldsymbol{u}} / \|A\hat{\boldsymbol{u}}\|$. The squeeze $\hat{\boldsymbol{v}}$ can be viewed as what is left from the squeeze $\hat{\boldsymbol{u}}$ after stripping off its component that

is responsible for rigid body movement. For a pure squeeze specified by $\rho\hat{\boldsymbol{v}}, \rho > 0$, we derive the resulting strain energy

$$U_p = \rho^2 \hat{\boldsymbol{u}}^T A \hat{\boldsymbol{u}} / (2\hat{\boldsymbol{u}}^T A A \hat{\boldsymbol{u}}). \tag{3.17}$$

While a stable squeeze makes sure that the movements of the two fingers do not contain any rigid body motion, a pure squeeze makes sure that the object deforms with no rigid body motion component. Figure 3.2 compares the effects of the unit stable squeeze $\hat{\boldsymbol{u}}$ and the unit pure squeeze $\hat{\boldsymbol{v}}$ on an object. While under $\hat{\boldsymbol{u}}$ the fingers drive the two contact points toward each other, under $\hat{\boldsymbol{v}}$ they bend the object to prevent any Euclidean motion, in a "smart" way by exerting smaller contact forces.

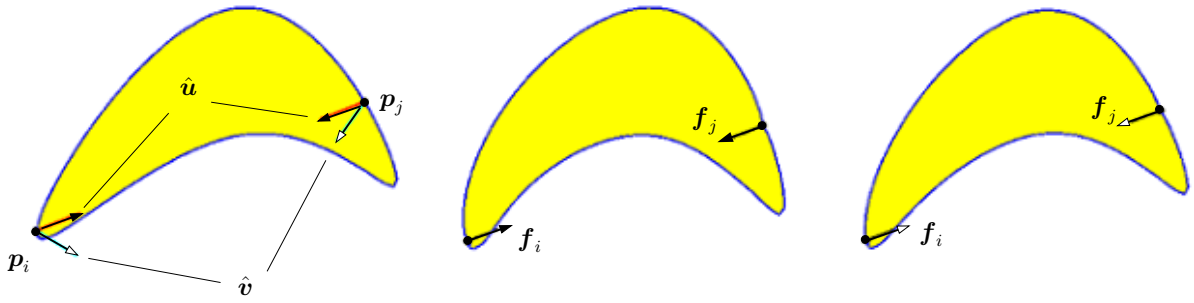

Figure 3.2 Comparison between unit stable and pure squeezes.

(a) original shape shown with a stable squeeze $\hat{\boldsymbol{u}} = (0.65923, 0.25577, -0.65923, -0.25577)^T$ in brown and a pure squeeze $\hat{\boldsymbol{v}} = (0.79644, -0.49167, -0.20702, -0.28477)^T$ in green; (b) deformed shape under $\hat{\boldsymbol{u}}$ with resulting contact forces $f_i = (0.90772, 0.35218)^T$ and $f_j = (0.90772, 0.35218)^T$; (c) deformed shape under $\hat{\boldsymbol{v}}$ with $f_i = (0.55243, 0.21433)^T$ and $f_j = (-0.55243, -0.21433)^T$.

Since translating two fingers $\mathcal{F}_1$ and $\mathcal{F}_2$ by $\boldsymbol{\delta}_i$ and $\boldsymbol{\delta}_j$, respectively, is equivalent to fixing one finger, say $\mathcal{F}_1$, while translating $\mathcal{F}_2$ by $\boldsymbol{\delta}_j - \boldsymbol{\delta}_i$ the two resulting configurations are identical except for a translation by $\boldsymbol{\delta}_i$. Thus, we consider a squeeze as stable(respectively, pure) if it is the same as $\rho\hat{\boldsymbol{u}}$(respectively, $\rho\hat{\boldsymbol{v}}$) up to translation and rotation.

CHAPTER 4. RESISTING AN ADVERSARY FINGER

In this chapter, we will consider adversary finger resistance. Consider a finger placement $\mathcal{G}(p_i, p_j)$ on a deformable object. Now that an adversary finger $\mathcal{A}$ comes in, makes contact with the object at p_k, and tries to break the grasp via a translation $\boldsymbol{a}$. To resist $\mathcal{A}$, the two grasping fingers $\mathcal{F}_1$ and $\mathcal{F}_2$ translate by $\boldsymbol{d}_1$ and $\boldsymbol{d}_2$ accordingly, respectively. We would like to find $\boldsymbol{d}_1$ and $\boldsymbol{d}_2$ that result in the minimum total effort by $\mathcal{F}_1$ and $\mathcal{F}_2$ in such resistance. The effort of resistance is best characterized as the total work performed by the two grasping fingers.

The general scenario is depicted in Figure 4.1, in which the finger contacts have evolved from the nodes p_i, p_j, p_k into segments as $\mathcal{F}_1$, $\mathcal{F}_2$, $\mathcal{A}$ translate. Every contact segment is uniquely represented by a set of nodes on it. Suppose that at one moment during the process, $\mathcal{F}_1$ makes contact with the set of nodes $\{\boldsymbol{p}_t \mid t \in \mathbb{I}\}$, $\mathcal{F}_2$ with $\{\boldsymbol{p}_t \mid t \in \mathbb{J}\}$, and $\mathcal{A}$ with $\{\boldsymbol{p}_t \mid t \in \mathbb{K}\}$. Some nodes (solid dots in the figure) are sticking on the fingertips, while others (hollow dots) are sliding. We can divide the scenario into small periods, such that within each period the contact index sets $\mathbb{I}$,$\mathbb{J}$,$\mathbb{K}$ do not change.

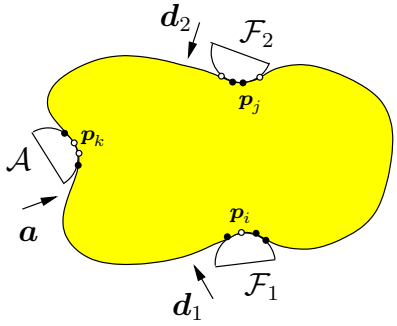

Figure 4.1 Grasp Resistance to a translating adversary finger $\mathcal{A}$.

We will approach this optimization problem in three steps. In Section 4.1, we will look at fixed point contacts (i.e., $|\mathbb{I}| = |\mathbb{J}| = |\mathbb{K}| = 1$ and the three sets never change) during the resistance. In Section 4.2, we will generalize the result to fixed segment contacts ($|\mathbb{I}| = |\mathbb{J}| = |\mathbb{K}| \geq 1$ and the sets do not vary). Based on this we will tackle the general situation with varying $\mathbb{I}$, $\mathbb{J}$, $\mathbb{K}$ and changing contact modes at individual nodes during the resistance under Coulomb friction in Section 4.3.

4.1 Fixed Point Contacts

The nodes $\boldsymbol{p}_i$, $\boldsymbol{p}_j$, and $\boldsymbol{p}_k$ will stay as the only contact points with the fingers $\mathcal{F}_1$, $\mathcal{F}_2$, and $\mathcal{A}$, respectively (as if the fingers and the object were glued together). Deformation of the object is due to their displacements

$$\bar{\boldsymbol{\delta}} = \begin{pmatrix} \boldsymbol{\delta}_i \\ \boldsymbol{\delta}_j \\ \boldsymbol{\delta}_k \end{pmatrix} = \begin{pmatrix} \boldsymbol{d}_i \\ \boldsymbol{d}_j \\ \boldsymbol{a} \end{pmatrix}. \tag{4.1}$$

By 3.10 the work done by $\mathcal{F}_1$ and $\mathcal{F}_2$ is

$$W_{\mathcal{F}} = \frac{1}{2} \begin{pmatrix} \boldsymbol{d}_1 \\ \boldsymbol{d}_2 \\ 0 \end{pmatrix}^T \bar{\boldsymbol{f}} = \frac{1}{2} \begin{pmatrix} \boldsymbol{d}_1 \\ \boldsymbol{d}_2 \\ 0 \end{pmatrix}^T C \begin{pmatrix} \boldsymbol{d}_1 \\ \boldsymbol{d}_2 \\ \boldsymbol{a} \end{pmatrix}. \tag{4.2}$$

Similarly, for the three point fingers we call $\bar{\boldsymbol{\delta}}$ a *stable resistance* if $\bar{\boldsymbol{\delta}} \in \text{col}(C)$, and a *pure resistance* if $\bar{\boldsymbol{\delta}} \in \text{col}(AC)$. Since m = 3, both col$(C)$ and col(AC) have three dimensions by Theorem 3.3.1.

4.1.1 Optimal stable resistance

Consider all $\boldsymbol{d}_1$ and $\boldsymbol{d}_2$ such that $\bar{\boldsymbol{\delta}} \in \text{col}(C)$, or equivalently, $\bar{\boldsymbol{\delta}} \perp \text{col}(B)$, which is spanned by $(1,0,1,0,1,0)^T$, $(0,1,0,1,0,1)^T$, and $(-y_i, x_i, -y_j, xj, -y_k, x_k)^T$. Equivalently, we require

$$\boldsymbol{d}_1 + \boldsymbol{d}_2 + \boldsymbol{a} = \boldsymbol{0}, \tag{4.3}$$

$$\boldsymbol{p}_i \times \boldsymbol{d}_1 + \boldsymbol{p}_j \times \boldsymbol{d}_2 + \boldsymbol{p}_k \times \boldsymbol{a} = 0, \tag{4.4}$$

Substitute equation 4.3 into 4.2 for $\boldsymbol{d}_2$, and rewrite $W_{\mathcal{F}}$ as a quadratic form in terms of $\boldsymbol{d}_1$:

$$W_{\mathcal{F}} = \frac{1}{2}\boldsymbol{d}_1^T H \boldsymbol{d}_1 + \boldsymbol{c}^T \boldsymbol{d}_1 + \omega, \tag{4.5}$$

where H, $\boldsymbol{c}$, and ω are constant matrix and vectors depending on $\boldsymbol{a}$ and C. It is easy to show that H is positive semi-definite.

Denote by $\hat{\boldsymbol{t}}$ the unit vector in the direction of $\boldsymbol{p}_i - \boldsymbol{p}_j$, and $\hat{\boldsymbol{n}}$ the unit vector such that $\hat{\boldsymbol{t}} \cdot \hat{\boldsymbol{n}} = 0$ and $\hat{\boldsymbol{t}} \times \hat{\boldsymbol{n}} = 1$. Write $\boldsymbol{d}_1 = \tau\hat{\boldsymbol{t}} + \eta\hat{\boldsymbol{n}}$. Substituting it and 4.3 into 4.4, we obtain

$$\eta = \boldsymbol{d} \cdot \hat{\boldsymbol{n}} = (\boldsymbol{p}_j - \boldsymbol{p}_k) \times \boldsymbol{a} / \|\boldsymbol{p}_i - \boldsymbol{p}_j\|. \tag{4.6}$$

Now, plug $\boldsymbol{d}_1 = \tau\hat{\boldsymbol{t}} + \eta\hat{\boldsymbol{n}}$ into 4.4. After a few steps, we have a new form for the work:

$$W_{\mathcal{F}} = \frac{1}{2}b_2\tau^2 + b_1\tau + b_0, \tag{4.7}$$

where $b_0 = \omega + \eta(\frac{1}{2}\eta\hat{\boldsymbol{n}}^T H + \boldsymbol{c}^T)$, $b_1 = (\eta\hat{\boldsymbol{n}}^T H + \boldsymbol{c}^T)\hat{\boldsymbol{t}}$, and $b_2 = \hat{\boldsymbol{t}}^T H \hat{\boldsymbol{t}}$. The positive semi-definiteness of H implies that $b_2 > 0$. Therefore, $W_{\mathcal{F}}$ is a parabola with the minimum value $W_{\mathcal{F}}^* = b_0 - \frac{b_1^2}{2b_2}$ achieved at $\tau = -b_1/b_2$. Note that b_0 scales with $\|a\|^2$ and b_1 scales with $\|a\|$, while b_2 is constant. The minimum work $W_{\mathcal{F}}^*$ scales quadratically with $\|a\|$.

Figure 4.2 shows a resistance scenario. The minimum work is $W_{\mathcal{F}}^* = 0.01031$. The average rotation per node is $\boldsymbol{\delta} \cdot \boldsymbol{v}_{2n} = 0.0035418$.

4.1.2 Optimal pure resistance

In this section we find a pure resistance that minimizes $W_{\mathcal{F}}$, considering only $\boldsymbol{d}_1$ and $\boldsymbol{d}_2$ such that $\bar{\boldsymbol{\delta}} \in \text{col}(AC)$. Represent $\bar{\boldsymbol{\delta}} = \tau_1\hat{\boldsymbol{u}}_1 + \tau_2\hat{\boldsymbol{u}}_2 + \tau_3\hat{\boldsymbol{u}}_3$, where $\hat{\boldsymbol{u}}_1$, $\hat{\boldsymbol{u}}_2$, $\hat{\boldsymbol{u}}_3$ are the

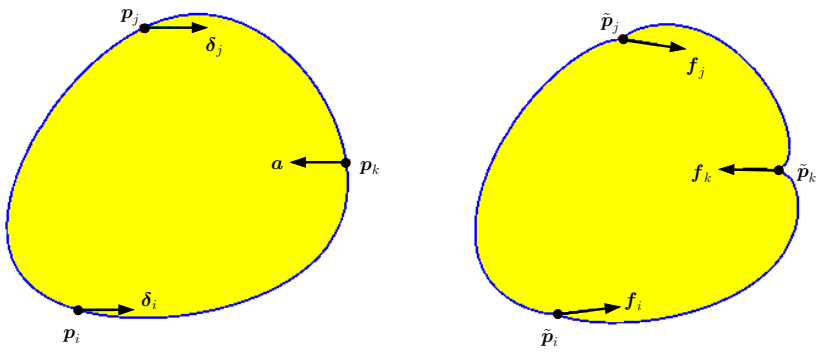

Figure 4.2 A grasp resisting an adversary finger.

A grasp $\mathcal{G}(\boldsymbol{p}_i,\ \boldsymbol{p}_j)$ resisting an adversary finger at $\boldsymbol{p}_k = (0.05900, 0.00502)^T$ under translation $\boldsymbol{\delta}_k = \boldsymbol{a} = (-0.01, 0)^T$, where $\boldsymbol{p}_i = (-0.03537, -0.04685)^T$ and $\boldsymbol{p}_j = (-0.01256, 0.05212)^T$: (a) undeformed shape marked with optimal displacements: $\boldsymbol{\delta}_i = (0.00475, 0.00006)^T$ and $\boldsymbol{\delta}_j = (0.00525, -0.00006)^T$; and (b) deformed shape marked with the corresponding nodal forces: $\boldsymbol{f}_i = (2.5031, 0.3105)^T$, $\boldsymbol{f}_j = (2.8792, -0.4901)^T$, and $\boldsymbol{f}_k = (-5.3823, 0.1796)^T$.

orthogonal unit vectors that span col(AC). From these two equivalent representations of $\bar{\boldsymbol{\delta}}$, we infer that

$$\boldsymbol{a} = Q \begin{pmatrix} \tau_1 \\ \tau_2 \\ \tau_3 \end{pmatrix}, \tag{4.8}$$

where the 2×3 matirx $Q = (\mathbf{0}, I_2)(\hat{\boldsymbol{u}}_1, \hat{\boldsymbol{u}}_2, \hat{\boldsymbol{u}}_3)$.

If Q is not of full rank and $\boldsymbol{a}$ is not in its column space, then we infer that $\bar{\boldsymbol{\delta}} \in$ col(AC) and the adversary finger cannot be resisted.

In the general case rank(Q) = 2, τ_2 and τ_3 are linear in τ_1, yielding $W_{\mathcal{F}}$ as a quadratic function of τ_1. The optimal grasping finger displacements can be obtained from $dW_{\mathcal{F}}/d\tau_1 = 0$. This solution also works for rank(Q) = 1 and $\boldsymbol{a} \in$ col(Q), after proper permutation of τ_1, τ_2, τ_3 to set the latter two to zero.

4.2 Fixed Segment Contacts

In this section, the contact index sets $\mathbb{I}$, $\mathbb{J}$, $\mathbb{K}$ may have sizes greater than one, but still they will not change during the resistance. In other words, no existing contacts will break and no new contacts will come in. All the nodes in contact with the same finger undergo the same displacement. More specifically, a contact node pt is displaced by

$$\boldsymbol{\delta}_t = \begin{cases} \boldsymbol{d}_1, & \text{if } t \in \mathbb{I}; \\ \boldsymbol{d}_2, & \text{if } t \in \mathbb{J}; \\ \boldsymbol{a}, & \text{if } t \in \mathbb{K}. \end{cases} \tag{4.9}$$

Rearrange the rows and columns of the reduced stiffness matrix in the same index order as in $\bar{\boldsymbol{\delta}}$.

Again, we first consider stable resistances, for which the following generalizations of 4.3 and 4.4 hold:

$$\sum_{t \in \mathbb{I} \cup \mathbb{J} \cup \mathbb{K}} \boldsymbol{\delta}_t = \boldsymbol{0} \quad \text{and} \quad \sum_{t \in \mathbb{I} \cup \mathbb{J} \cup \mathbb{K}} \boldsymbol{p}_t \times \boldsymbol{\delta}_t = 0. \tag{4.10}$$

The first condition above yields $\boldsymbol{d}_2$ in terms of $\boldsymbol{d}_1$ and $\boldsymbol{a}$. Substitute it into the second condition to yield

$$|\mathbb{I}|(\breve{\boldsymbol{p}} - \breve{\boldsymbol{q}}) \times \boldsymbol{d}_1 + |\mathbb{K}|(\breve{\boldsymbol{r}} - \breve{\boldsymbol{q}}) \times \boldsymbol{a} = 0, \tag{4.11}$$

where $\breve{\boldsymbol{p}} = \frac{1}{|\mathbb{I}|} \sum_{t \in \mathbb{I}} \boldsymbol{p}_t$, $\breve{\boldsymbol{q}} = \frac{1}{|\mathbb{J}|} \sum_{t \in \mathbb{J}} \boldsymbol{p}_t$, and $\breve{\boldsymbol{r}} = \frac{1}{|\mathbb{K}|} \sum_{t \in \mathbb{K}} \boldsymbol{p}_t$ are referred to as the *contact centroids* of the fingers $\mathcal{F}_1$,$\mathcal{F}_2$,$\mathcal{A}$, respectively.

$\mathcal{F}_1$ and $\mathcal{F}_2$ into the form of equation 4.5, where H, $\boldsymbol{c}$, and ω assume new expressions. Minimization parallels that in Section 4.1 with a decomposition of $\boldsymbol{d}_1$ along the direction $\hat{\boldsymbol{t}}$ of $\breve{\boldsymbol{p}} - \breve{\boldsymbol{q}}$, and its orthogonal direction $\hat{\boldsymbol{n}}$.

The case of a pure resistance with fixed segment contacts also generalizes that of fixed point contacts in Section 4.1. We will end up with a very similar optimization

problem. Aside from a different form of $W_{\mathcal{F}}$ and different variables τ_1', τ_2', τ_3', over which the constraint is $\boldsymbol{a} = (\mathbf{0}, I_2)(\hat{\boldsymbol{u}}_1', \hat{\boldsymbol{u}}_2', \hat{\boldsymbol{u}}_3')(\tau_1', \tau_2', \tau_3')^T$.

4.3 Frictional Segment Contacts

We are now finally ready to consider optimal resistance with varying segment contacts under friction. The two grasping fingers and the adversary finger have semicircular fingertips with possibly different radii. In a realistic scenario, the grasping fingers $\mathcal{F}_1$ and $\mathcal{F}_2$ first perform a squeeze on the object by translating toward each other via $s(\boldsymbol{p}_j - \boldsymbol{p}_i)$ and $s(\boldsymbol{p}_i - \boldsymbol{p}_j)$, for some $s > 0$, which is called the *pre-grasp*. Then the adversary finger $\mathcal{A}$ makes contact at the node $\boldsymbol{p}_k$ and exerts a translation $\boldsymbol{a}$ to try to break the grasp. The system configuration right before this disturbance, including the objects deformed shape and the contact index sets $\mathbb{I}$ and $\mathbb{J}$ for $\mathcal{F}_1$ and $\mathcal{F}_2$, can be determined using the event-based squeeze grasping algorithm from (3).

The translation distance by the adversary finger $\mathcal{A}$ will be sequenced into $a_0 = 0 < a_1 < \cdots < |\boldsymbol{a}|$ such that at every a_l , one of the four contact events A, B, C, and D described in (3) takes place.

Algorithm 1 describes how $\mathcal{F}_1$ and $\mathcal{F}_2$ resist $\mathcal{A}$. Again, denote by $\mathbb{I}$, $\mathbb{J}$, $\mathbb{K}$ the sets of indices of the nodes that are in contact with $\mathcal{F}_1$, $\mathcal{F}_2$, and $\mathcal{A}$, respectively.

Algorithm 1 Resisting a Translating Adversary Finger under Frictional Segment Contact

Input: contact index sets $\mathbb{I}$, $\mathbb{J}$,$\mathbb{K}$ for $\mathcal{F}_1$, $\mathcal{F}_2$, $\mathcal{A}$, translation a of $\mathcal{F}_2$

1: $a \leftarrow 0$

2: let $\mathbb{I}$, $\mathbb{J}$,$\mathbb{K}$ contain the indices of the initial point contacts with $\mathcal{F}_1$, $\mathcal{F}_2$, $\mathcal{A}$, respectively

3: initialize $\mathbb{T}$ and $\mathbb{P}$

4: **while** $a < \|\boldsymbol{a}\|$ and no finger slips do **do**

5: construct the form of $\tilde{W}'_{\mathcal{F}}$ based on equations 4.12, 4.13, and $\mathbb{I}$, $\mathbb{J}$,$\mathbb{K}$

6: minimize $\tilde{W}'_{\mathcal{F}}$ to obtain ψ_1 and ψ_2 as the translations of $\mathcal{F}_1$ and $\mathcal{F}_1$ in response to a (hypothesized) unit translation $a/\|\boldsymbol{a}\|$ by $\mathcal{A}$.

7: execute the event-driven algorithm in (3) along the displacement directions computed in step 6 until the next contact event occurs

8: compute the actual work $W'_{\mathcal{F}}$

9: $W_{\mathcal{F}} \leftarrow W_{\mathcal{F}} + W'_{\mathcal{F}}$

10: update $\mathbb{I}$, $\mathbb{J}$, $\mathbb{K}$, $\mathbb{T}$, $\mathbb{P}$ according to the contact event

11: update the contact force $\boldsymbol{f}_t, \forall\ t \in \mathbb{I} \cup \mathbb{J} \cup \mathbb{K}$

12: **end while**

13: **if** $a < \|\boldsymbol{a}\|$ and ($\mathcal{F}_1$ or $\mathcal{F}_2$ slips) **then**

14: **return** failure

15: **else**

16: **return** $W_{\mathcal{F}}$

17: **end if**

Consider the moment when $\mathcal{A}$ has translated by the distance a_l. For a contact node $\boldsymbol{p}_t$ we use $\boldsymbol{\delta}_t^{(l)}$, $\boldsymbol{f}_t^{(l)}$, and $\theta_t^{(l)}$ to refer to its displacement, contact force, and polar angle with respect to the center of its contacting fingertip.

Next, $\mathcal{A}$ will continue moving by an extra distance ξ in the direction of $\boldsymbol{a}$. Suppose that ξ is small enough such that all contacts and their modes will not change. We

determine the extra translations $\boldsymbol{d}'_1$ of $\mathcal{F}_1$ and $\boldsymbol{d}'_2$ of $\mathcal{F}_2$ to resist this extra movement by $\mathcal{A}$, via minimizing the extra work performed by these two fingers:

$$W'_{\mathcal{F}} = \sum_{t\in\mathbb{I}\cup\mathbb{J}} \boldsymbol{\delta}'_t \boldsymbol{f}_t^{(l)} + \frac{1}{2}\sum_{t\in\mathbb{I}\cup\mathbb{J}} \boldsymbol{\delta}'_t \boldsymbol{f}'_t \tag{4.12}$$

In the above, for $t \in \mathbb{I}\cup\mathbb{J}$, $\boldsymbol{\delta}'_t$ is the change in the displacement of the contact node $\boldsymbol{p}_t$ from $\boldsymbol{\delta}_t^{(l)}$, and $\boldsymbol{f}'_t$ the change in its contact force from $\boldsymbol{f}_t^{(l)}$.

During this extra translation period, if a node $\boldsymbol{p}_t$, $t \in \mathbb{I}\cup\mathbb{J}$, sticks, then $\boldsymbol{\delta}'_t = \boldsymbol{d}'_1$ or $\boldsymbol{d}'_2$. If it slides, then $\boldsymbol{\delta}'_t$ will be the sum of $\boldsymbol{d}'_1$ or $\boldsymbol{d}'_2$ and the nodes movement $r\begin{pmatrix}\cos\theta_t - \cos\theta_t^{(l)}\\ \sin\theta_t - \sin\theta_t^{(l)}\end{pmatrix}$, on the tip of $\mathcal{F}_1$ or $\mathcal{F}_2$ that it is in contact with. Minimization of $W'_{\mathcal{F}}$ would be over $\boldsymbol{\delta}'_1$ and $\boldsymbol{\delta}'_2$, and the polar angle θ_t of every sliding contact $\boldsymbol{p}_t$. It could get too inefficient.

We stipulate that the work performed on $\boldsymbol{p}_t$, $t \in \mathbb{I}\cup\mathbb{J}$, due to its sliding, by the contacting finger $\mathcal{F}_1$ or $\mathcal{F}_2$ will be significantly less than the amount due to its translation with the finger. Instead of minimizing $W'_{\mathcal{F}}$, we minimize its approximation $\tilde{W}'_{\mathcal{F}}$ by treating every sliding node in contact with $\mathcal{F}_1$, $\mathcal{F}_2$, or $\mathcal{A}$ as if it would be sticking during the period of the extra resistance period.

In short, whether a contact node $\boldsymbol{p}_t$ sticks or slips, its extra displacement $\boldsymbol{\delta}'_t$ will be set as follows:

$$\boldsymbol{\delta}_t = \begin{cases} \boldsymbol{d}'_1, \text{ if } t \in \mathbb{I};\\ \boldsymbol{d}'_2, \text{ if } t \in \mathbb{J};\\ \xi\hat{\boldsymbol{a}}, \text{ if } t \in \mathbb{K}. \end{cases} \tag{4.13}$$

Then $\boldsymbol{d}_1 = \xi\boldsymbol{\psi}_1$ and $\boldsymbol{d}'_2 = \xi\boldsymbol{\psi}_2$, where $\boldsymbol{\psi}_1$ and $\boldsymbol{\psi}_2$ are determined like $\boldsymbol{d}_1$ and $\boldsymbol{d}_2$ in Section 4.2 with $\hat{\boldsymbol{a}}$ replacing $\boldsymbol{a}$.

We determine the extra distance ξ by which $\mathcal{A}$ translates until the next contact event happens, by using the event-driven algorithm proposed in (3). Once an event occurs, the overall translation distance for $\mathcal{A}$ is updated as $a_{l+1} = a_l + \xi$. In addition to the index sets $\mathbb{I}$, $\mathbb{J}$, $\mathbb{K}$, update the set $\mathbb{P}$ of sliding contacts and the set $\mathbb{T}$ of sticking contacts. If

Table 4.1 Forces exerted and work performed by the the two grasping fingers in Figure 4.3 under translations $\boldsymbol{d}_1$, $\boldsymbol{d}_2$, and $\boldsymbol{a}$.

	$\mathcal{F}_1$	$\mathcal{F}_2$
force(start)	2.098	-2.566
force(end)	8.136	-1.23
work	0.0101	-0.0015

the adversary finger $\mathcal{A}$ begins to slip after an event, it has been successfully resisted. If either $\mathcal{F}_1$ or $\mathcal{F}_2$ starts to slide, the grasp fails to resist $\mathcal{A}$. If none of the above two cases happens, $\mathcal{A}$ will complete its translation $\boldsymbol{a}$ while being resisted.

4.4 Simulation and Experiment on Grasp Resistance

Figure 4.3(a) shows an object with convex shape grasped under a stable squeeze by $\mathcal{F}_1$ (translating via $(0.00068, 0.002)^T$ from p_i to p_j) and $\mathcal{F}_2$ (motionless). Then, an adversary finger $\mathcal{A}$ starts pushing the object through translation $\boldsymbol{a} = (0.0024, 0.0044)^T$, as shown in (b). All three fingertips have radius 0.02. Algorithm 1 generates two trajectories for $\mathcal{F}_1$ and $\mathcal{F}_2$ for a stable squeeze shown in (c). They have total displacements $\boldsymbol{d}_1 = (-0.0008, -0.0019)^T$ and $\boldsymbol{d}_2 = (-0.0007, -0.0005)^T$. Table 4.1 displays the components of the finger forces exerted along the translation directions, at the start and the end of resistance, and the work performed by the fingers. A negative force reading on $\mathcal{F}_2$ indicates that the contact force influenced by friction was pulling away from the translation direction of the finger. Contact events A, B, C, D occurred 7, 0, 3, and 2 times, respectively, during the resistance. The coefficient of contact friction is 0.4.

Shown in Figure 4.4(a) is an experiment to validate the results in Table 4.1 from the instance in Figure 4.3. The object with exactly the same shape in Figure 4.3 was placed on a raised platform. The grasping fingertips $\mathcal{F}_1$ and $\mathcal{F}_2$ were respectively controlled by an Adept Cobra 600 manipulator and the Barrett Hand. As shown in (b), $\mathcal{F}_1$ was

attached to a force meter from Ametek Hunter Spring, which was connected to the Adept's open end via an adapter. The manipulator has an accuracy of 0.02mm in any horizontal direction. Since none of the three fingers of the Barrett Hand could be controlled to perform straight line motions, we let its middle finger push fingertip $\mathcal{F}_2$ via a linear mechanism, which is shown in (c) in both top-down and side views. The mechanism was an aluminum cylindrical stick constrained by ball bearings embedded inside two boxes. At its one end was a disk to be pushed by the finger of the Barrett Hand or human hand. Near its other end, a force meter was attached underneath. The tip $\mathcal{F}_2$ was mounted at the front of the force meter, which would be able to measure the force exerted by the tip once it made contact with the object.

The human hand pushed the adversary fingertip $\mathcal{A}$ via another linear mechanism identical to the one driving $\mathcal{F}_2$. No force meter was attached to this pusher. A ruler was mounted on the tops of the two ball bearing boxes to measure the travel distance by $\mathcal{A}$. The translations by $\mathcal{F}_1$ and $\mathcal{F}_2$, meanwhile, were precisely controlled by the Adept and the Barrett Hand. The fingers $\mathcal{F}_1$ and $\mathcal{F}_2$ first made contact with a foam object. To repeat the simulation instance in the above, $\mathcal{F}_2$ stayed still and $\mathcal{F}_1$ squeezed the object via a translation $(-0.00068, 0.002)^T$ along the line through their initial contact points with the object. The configuration after the squeeze is shown in Figure 4.5(a). Afterward, the human hand pushed $\mathcal{A}$ via the linear mechanism to complete a translation $\boldsymbol{a} = (0.0024, 0.0044)^T$. Algorithm 1 generated two trajectories shown in Figure 4.3(c) respectively for $\mathcal{F}_1$ and $\mathcal{F}_2$ based on stable squeezes. For ease of control, each trajectory was straightened by connecting its starting location to its final location, yielding translations $\boldsymbol{d}_1 = (-0.0008, -0.0019)^T$ and $\boldsymbol{d}_2 = (-0.0007, -0.0005)^T$ (see the dashed lines in Figure 4.3(c)). The human hand executed the push $\boldsymbol{a}$, which was simultaneously being resisted by the Adept arm and the Barrett hand via translations $\boldsymbol{d}_1$ and $\boldsymbol{d}_2$, respectively.

We refer to the resistance specified by $\boldsymbol{d}_1$ and $\boldsymbol{d}_2$ as the "optimal" resistance. The

Table 4.2 Forces exerted and work performed by $\mathcal{F}_1$ and $\mathcal{F}_2$ in Figure 4.5 under $\boldsymbol{d}_1$ and $\boldsymbol{d}_2$ computed by the resistance algorithm (columns 23) or arbitrarily chosen (columns 45).

	"optimal" resist.		"arbitrary" resist.	
	$\mathcal{F}_1$	$\mathcal{F}_2$	$\mathcal{F}_1$	$\mathcal{F}_2$
force(start)	2.22	-2.67	7.05	4.20
force(end)	8.06	-1.45	14.86	13.93
work	0.0107	-0.0017	0.0463	0.0328

work done by $\mathcal{F}_1$ or $\mathcal{F}_2$ was estimated as half the product of the translation distance with the summation of the initial and final force readings for each finger. Columns 2 and 3 in Table 4.2 displayed the force readings on these two grasping fingers at the start and the end of the resistance, and the work they performed. We can see that small discrepancies exist compared to Table 4.1. They were mainly due to the trajectory straightening and measurement errors in the experiment. For comparison, we also tested an "arbitrary" resistance strategy against the same adversary finger disturbance. We arbitrarily chose a translation direction $\boldsymbol{d}_2/\|\boldsymbol{d}_2\| = (0.447, -0.894)^T$ for $\mathcal{F}_2$. Then $\boldsymbol{d}_1 = (-0.004, -0.0012)^T$ and $\boldsymbol{d}_2 = (0.0016, -0.0032)^T$ were determined from the condition $(\boldsymbol{d}_1^T, \boldsymbol{d}_2^T, \boldsymbol{a}^T)^T \perp \text{col}(B)$ for a stable squeeze. The experimental result was included in Table 4.2. It can be seen that much less work was carried out by $\mathcal{F}_1$ and $\mathcal{F}_2$ under the optimal resistance strategy.

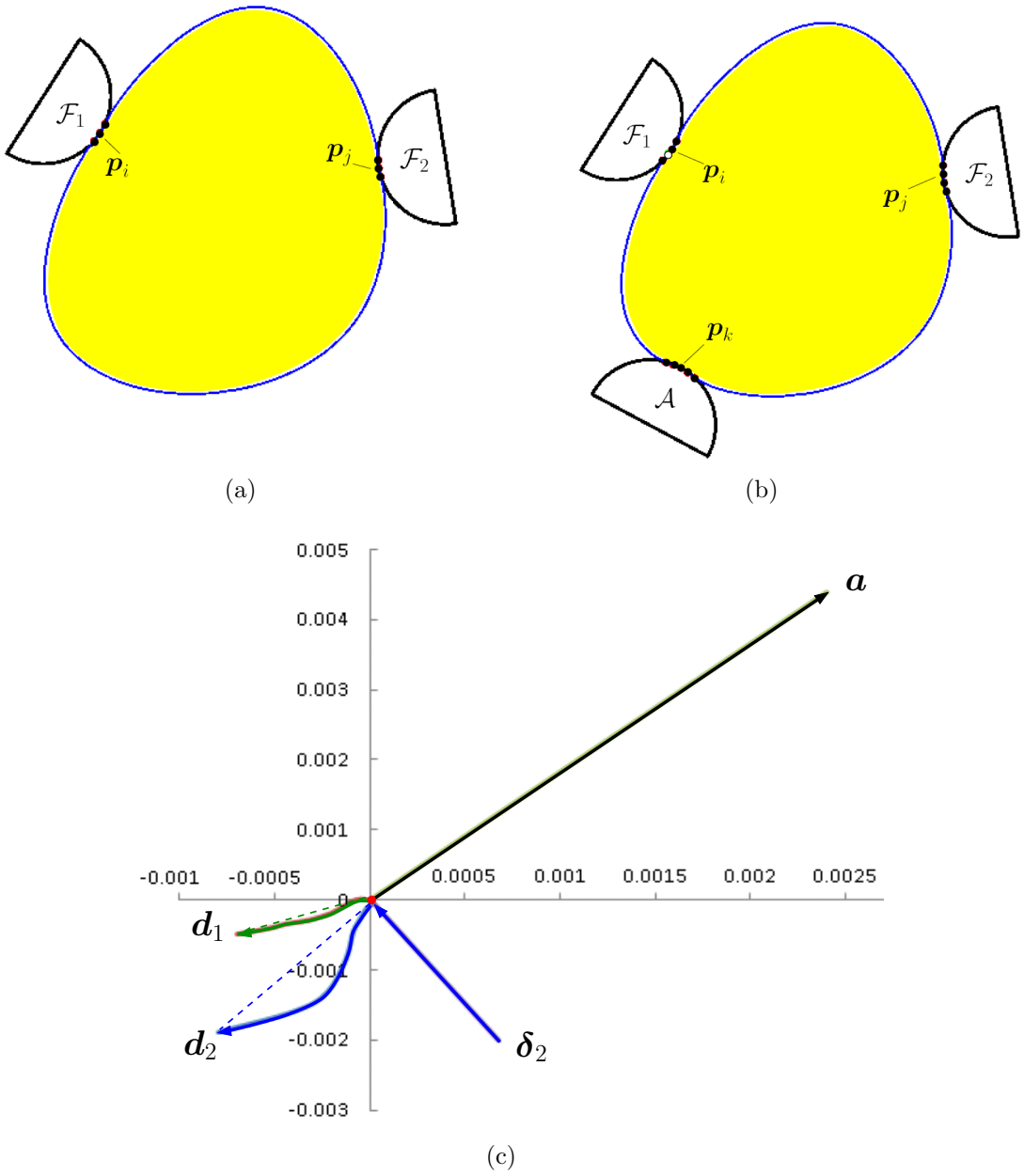

Figure 4.3 Resisting an adversary semicircular fingertip under friction.

(a) A convex shape grasped via a stable squeeze. (b) Successful resistance to an adversary finger $\mathcal{A}$. (c) Trajectories of the three fingers during the resistance, with their starting points translated to coincide with the origin, which, for display purpose, is also made the ending point of the trajectory $\boldsymbol{\delta}_1$ of $\mathcal{F}_1$ in achieving an initial grasp before the resistance.

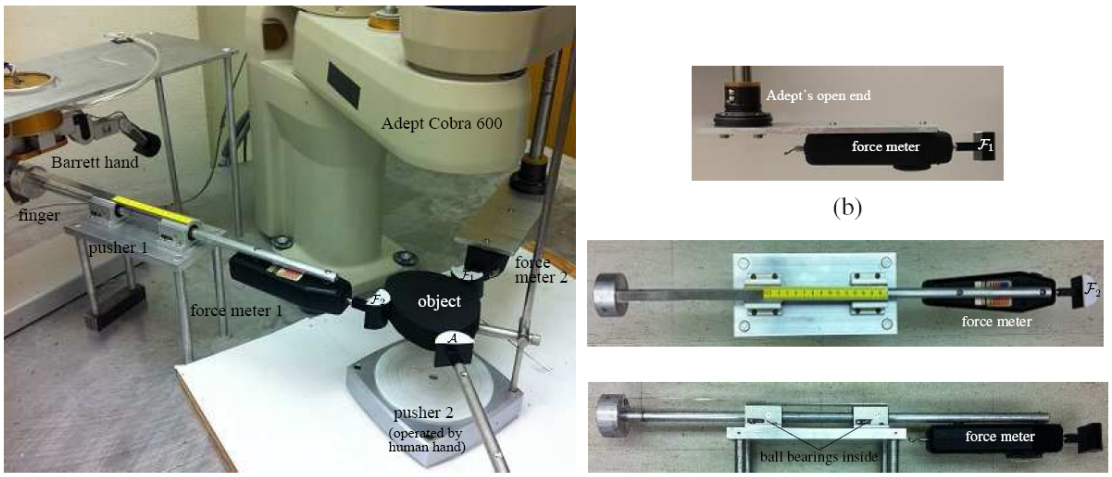

Figure 4.4 Experimental setup for resisting an adversary fingertip $\mathcal{A}$.

(a) grasping fingertips $\mathcal{F}_1$ and $\mathcal{F}_2$ driven by an Adept Cobra 600 manipulator and a finger of the Barrett hand, respectively, and $\mathcal{A}$ by the human hand; (b) $\mathcal{F}_1$ attached to a force meter rigidly connected to the Adept's open end via an adapter; (c) $\mathcal{F}_2$ attached to another force meter rigidly connected to a linear mechanism to be pushed by the Barrett finger.

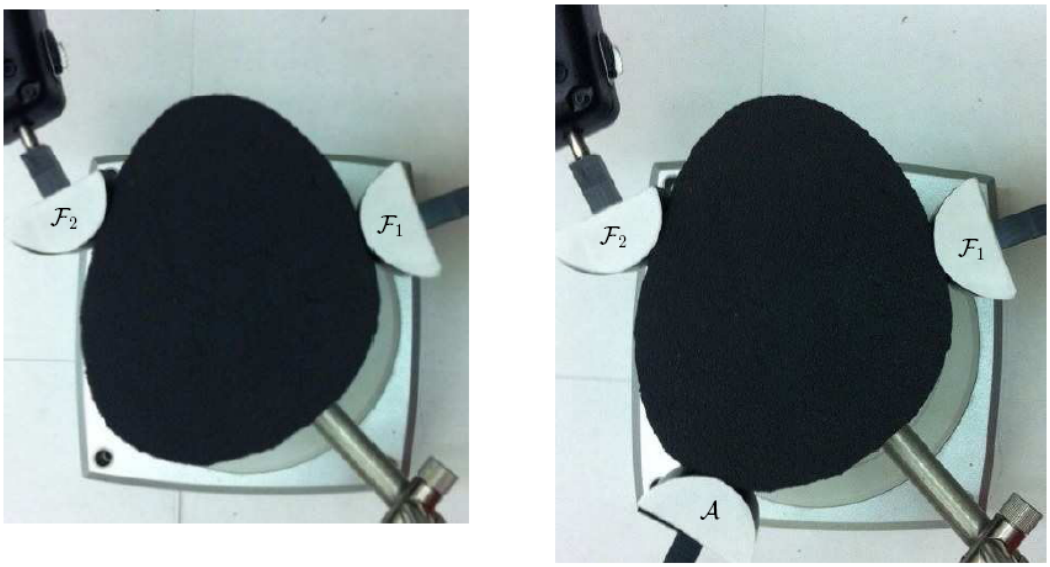

(a) (b)

Figure 4.5 Experiment for resisting an adversary finger.

(a) Grasp of a convex object and (b) its resistance to an adversary finger $\mathcal{A}$. The translation $\boldsymbol{\delta}_1$ of $\mathcal{F}_1$ in (a), and the translations $\boldsymbol{d}_1$, $\boldsymbol{d}_2$, and $\boldsymbol{a}$ of $\mathcal{F}_1$,$\mathcal{F}_2$ and $\mathcal{A}$ are drawn in Figure 4.3.

CHAPTER 5. PICKING UP 3D SOFT OBJECTS

This chapter will begin with a brief review of linear elasticity for 3D solids, and the characterization of all displacement fields that represent rigid body movements. It will then describe an FEM formulation of deformation under gravity. We will move on to offer a solution of the deformed shape of a solid from specified contact displacements. Finally we will propose a strategy to pick up a deformable 3D object with two fingers under resting.

5.1 Linear Elasticity

Consider a 3D object under a displacement field $(u(x,y,z), v(x,y,z), w(x,y,z))^T$. Every point $(x,y,z)^T$ inside the object moves to $(x+u, y+v, z+w)^T$. Denote by ϵ_x, ϵ_y, ϵ_z the normal strains along the x-, y-, and z-directions, respectively, and γ_{xy}, γ_{xz}, γ_{yz} the shear strains in the xy-, xz-, and yz-planes, respectively. They are given below:

$$\begin{aligned}
\epsilon_x &= \frac{\partial u}{\partial x}, \\
\epsilon_y &= \frac{\partial v}{\partial y}, \\
\epsilon_z &= \frac{\partial w}{\partial z}, \\
\gamma_{xy} &= \frac{\partial u}{\partial y} + \frac{\partial v}{\partial x}. \\
\gamma_{xz} &= \frac{\partial u}{\partial z} + \frac{\partial w}{\partial x}. \\
\gamma_{yz} &= \frac{\partial w}{\partial y} + \frac{\partial v}{\partial z}.
\end{aligned} \tag{5.1}$$

The strain energy of the object can be derived:

$$U = \frac{E}{2(1+\nu)} \int_V ((\epsilon_x^2 + \epsilon_y^2 + \epsilon_z^2) + \frac{\nu}{(1-2\nu)}(\epsilon_x + \epsilon_y + \epsilon_z)^2 + \frac{1}{2}(\gamma_{xy}^2 + \gamma_{xz}^2 + \gamma_{yz}^2))dV. \quad (5.2)$$

where E and ν are Young's modulus and Poisson's ratio of the material, respectively, with $E > 0$ and $-1 < \nu < \frac{1}{2}$ for most materials including those considered in our grasping task.

Theorem 5.1.1. *Under linear elasticity, any displacement field* $(u, v, w)^T$ *that yields zero strain energy is linearly spanned by the following six fields:*

$$\begin{pmatrix} 1 \\ 0 \\ 0 \end{pmatrix}, \begin{pmatrix} 0 \\ 1 \\ 0 \end{pmatrix}, \begin{pmatrix} 0 \\ 0 \\ 1 \end{pmatrix}, \begin{pmatrix} 0 \\ -z \\ y \end{pmatrix}, \begin{pmatrix} z \\ 0 \\ -x \end{pmatrix}, \begin{pmatrix} -y \\ x \\ 0 \end{pmatrix}.$$

The first three displacement fields in the theorem represent unit translations in the x-, y-, and z-directions, respectively. The next three fields represent rotations about the x-, y-, and z-axes under linear elasticity, respectively.

5.2 The Finite Element Method with Gravity

We represent a solid as a tetrahedral mesh with n vertices $\boldsymbol{p}_1$, ..., $\boldsymbol{p}_n$, where $\boldsymbol{p}_i = (x_i, y_i, z_i)^T$, for $1 \leq i \leq n$.

Similar as in the planar case, we infer from Theorem 5.1.1 that the stiffness matrix has a null space spanned by the following six $3n$-vectors:

$$\begin{aligned} \boldsymbol{t}_x &= (1, 0, 0, 1, 0, ..., 0)^T, \\ \boldsymbol{t}_y &= (0, 1, 0, 0, 1, ..., 0)^T, \\ \boldsymbol{t}_z &= (0, 0, 1, 0, 0, ..., 1)^T, \\ \boldsymbol{r}_x &= (0, -z_1, y_1, 0, -z_2, ..., y_n)^T, \\ \boldsymbol{r}_y &= (z_1, 0, x_1, z_2, 0, ..., -x_n)^T, \\ \boldsymbol{r}_z &= (-y_1, x_1, 0, -y_2, x_2, ..., 0)^T. \end{aligned} \quad (5.3)$$

On the 3D grasping, the gravitational force can rarely be ignored since it plays an important role during the deformation. Assume that the mass is uniformly distributed inside the body. Thus every element has mass proportional to its volume.We assign the element's mass evenly to its four vertices. Thus the total gravitational force exerted on a vertex $\boldsymbol{p}_i$, $1 \leq i \leq n$, sums up a quarter of the gravitational force on each tetrahedron it is incident on. Write all nodal gravitation forces into a vector $\boldsymbol{G}$. It is straightforward to verify that $\boldsymbol{G}$ is orthogonal with all the six vectors spanning the null space except $\boldsymbol{t}_z$, with which it has a dot product $-mg$, where m is the object's mass and $g = 9.8$ is the gravitational acceleraton.

The potential energy of the system can be represented as

$$\Pi = \frac{1}{2}\boldsymbol{\Delta}^T K \boldsymbol{\Delta} - \boldsymbol{\Delta}^T(\boldsymbol{F} + \boldsymbol{G}). \tag{5.4}$$

At equilibrium, it reaches its minimum value, implying

$$K\boldsymbol{\Delta}^T = \boldsymbol{F} + \boldsymbol{G}. \tag{5.5}$$

The stiffness matrix K is symmetric and thus diagonalizable. With $3n$ independent eigenvectors, it is also known to be positive semi-definite. Given its six-dimensional null space, K has $3n-6$ positive eigenvalues λ_1, ..., λ_{3n-6} corresponding to unit eigenvectors $\boldsymbol{v}_1$, ..., $\boldsymbol{v}_{3n-6}$. Let $\boldsymbol{v}_{3n-5}$, $\boldsymbol{v}_{3n-4}$, $\boldsymbol{v}_{3n-3}$ be normalized over $\boldsymbol{t}_x$, $\boldsymbol{t}_y$, $\boldsymbol{t}_z$, respectively. And let $\boldsymbol{v}_{3n-2}$, $\boldsymbol{v}_{3n-1}$, $\boldsymbol{v}_{3n}$ be orthogonalized over $\boldsymbol{r}_x$, $\boldsymbol{r}_y$, $\boldsymbol{r}_z$ using Gram-Schmidt procedure. Thus, $\boldsymbol{G} \cdot \boldsymbol{v}_{3n-3} = -mg/\sqrt{n}$ while $\boldsymbol{G} \cdot \boldsymbol{v}_j = 0$, $3n-5 \leq j \leq 3n$ and $j \neq 3n-3$. The matrix has a spectral decomposition $K = V\Lambda V^T$, where $V = (\boldsymbol{v}_1, ..., \boldsymbol{v}_{3n})$ and $\Lambda = diag(\lambda_1, ..., \lambda_{3n-6}, 0, ..., 0)$.

Because of the singularity of K, boundary conditions are required for solution of 5.5. They will come from the displacements of the contact nodes as they move with the squeezing fingers or stay with the supporting plane.

5.3 Deformation from Specified Contact Displacements

The set of contact nodes will not vary during a very small period of squeeze on the solid by the fingers. First we need to compute the deformation of the 3D object from specified displacements $\boldsymbol{\delta}_{i1}$, ..., $\boldsymbol{\delta}_{im}$ of some boundary nodes $\boldsymbol{p}_{i1}$, ..., $\boldsymbol{p}_{im}$, which are supposed to be in contact with a grasping finger or the supporting plane. We refer to the set $\mathbb{C} = \{i_1, ..., i_m\}$ as the contact index set. Zero external forces are applied at the non-contact nodes, that is, $\boldsymbol{f}_k = 0$, for $k = 1, ..., n$ and $k \notin \mathbb{C}$.

Denote $\bar{\boldsymbol{\Delta}} = (\boldsymbol{\delta}_{i1}^T, ..., \boldsymbol{\delta}_{im}^T)^T$ as before. We can solve for the contact force vector $\bar{\boldsymbol{F}}$ and the displacement field $\boldsymbol{\Delta}$ from $\bar{\boldsymbol{\Delta}}$ by performing a procedure similar to the one in (3). Substitute $K = V\Lambda V^T$ into 5.5, and left multiply both sides of the resulting equation with V^T . This yields

$$\begin{aligned} \boldsymbol{\Delta} &= \sum_{k=1}^{3n-6} \frac{1}{\lambda_k}(\boldsymbol{v}_k^T(\boldsymbol{F}+\boldsymbol{G}))\boldsymbol{v}_k + (\boldsymbol{v}_{3n-5}, ..., \boldsymbol{v}_{3n})\boldsymbol{b} \\ &= \sum_{k=1}^{3n-6} \frac{1}{\lambda_k}(\bar{\boldsymbol{v}}_k^T\bar{\boldsymbol{F}})\boldsymbol{v}_k + (\boldsymbol{v}_{3n-5}, ..., \boldsymbol{v}_{3n})\boldsymbol{b} + \boldsymbol{D}, \end{aligned} \tag{5.6}$$

where $\boldsymbol{D} = \sum_{k=1}^{3n-6} \frac{1}{\lambda_k}(\boldsymbol{v}_k^T\boldsymbol{G})\boldsymbol{v}_k$ is a constant vector. The $3m$ equations for $\boldsymbol{\delta}_{i1}, ..., \boldsymbol{\delta}_{im}$ are extracted from 5.6, and combined with the six equations $\boldsymbol{v}_k^T(\boldsymbol{F}+\boldsymbol{G}) = 0$, $k = 3n-5$, ..., $3n$. This sets up a linear equation in $\bar{\boldsymbol{F}}$ and $\boldsymbol{b}$:

$$M \begin{pmatrix} \bar{\boldsymbol{F}} \\ \boldsymbol{b} \end{pmatrix} = \begin{pmatrix} \bar{\boldsymbol{\Delta}} - \bar{\boldsymbol{D}} \\ (0, 0, mg/\sqrt{n}, 0, 0, 0)^T \end{pmatrix}, \tag{5.7}$$

where

$$M = \begin{pmatrix} A & B \\ B^T & 0 \end{pmatrix}, \tag{5.8}$$

with the $3m \times 3m$ matrix $A = \sum_{k=1}^{3n-6} \frac{1}{\lambda_k}(\bar{\boldsymbol{v}}_k\bar{\boldsymbol{v}}_k^T$ and the 6×6 matrix $B = (\bar{\boldsymbol{v}}_{3n-5}, ..., \bar{\boldsymbol{v}}_{3n})$.

Theorem 5.3.1. *The matrix M is non-singular if and only if the m contact points are not collinear.*

Under the above theorem, when the contacts are not collinear, the system 5.7 has a unique solution, in other words, the deformation is uniquely determined. To solve the system, we invert the matrix M to obtain

$$M^{-1} = \begin{pmatrix} C & E \\ E^T & H \end{pmatrix}, \tag{5.9}$$

where C, E, and H are matrices of dimensions $3m \times 3m$, $3m \times 6$, and 6×6, respectively. Left multiplication of M^{-1} with both sides of 5.7 yields

$$\begin{aligned} \bar{\boldsymbol{F}} &= C(\bar{\boldsymbol{\Delta}} - \bar{\boldsymbol{D}}) - E(0, 0, mg/\sqrt{n}, 0, 0, 0)^T \\ &= C(\bar{\boldsymbol{\Delta}} - \bar{\boldsymbol{D}}) - \frac{mg}{\sqrt{n}}\boldsymbol{e}_3, \end{aligned} \tag{5.10}$$

where $\boldsymbol{e}_3$ is the third column of E. The equation relates the contact forces to the specified contact displacements. With $\boldsymbol{F}$ and $\boldsymbol{D}$ determined, the displacement vector follows from 5.7.

5.4 Grasping to Pick up a Solid

Having studied deformation under contacts, we move on to consider the task of using two fingers to pick up a deformable 3D solid on a horizontal plane $\mathcal{P}$. The object's initial resting configuration is determined from a surface triangle $\triangle \boldsymbol{p}_q \boldsymbol{p}_r \boldsymbol{p}_s$ in contact with $\mathcal{P}$ onto which the vertical projection of the object's center of mass lies in the interior of the triangle. The object deforms under gravity over the triangle, causing the contact region to grow from $\triangle \boldsymbol{p}_q \boldsymbol{p}_r \boldsymbol{p}_s$.

The fingers have identical hemispherical tips $\mathcal{F}_1$ and $\mathcal{F}_2$ for simplicity and make initial contact with the resting object at the nodes $\boldsymbol{p}_i$ and $\boldsymbol{p}_j$ in their current locations displaced under gravity(as shown in Figure 5.1(a)). Then the fingertips squeeze the object(as shown in Figure 5.1(b)) and later lift it up via a vertically upward translation, breaking its contact with the plane as in Figure 5.1(c).

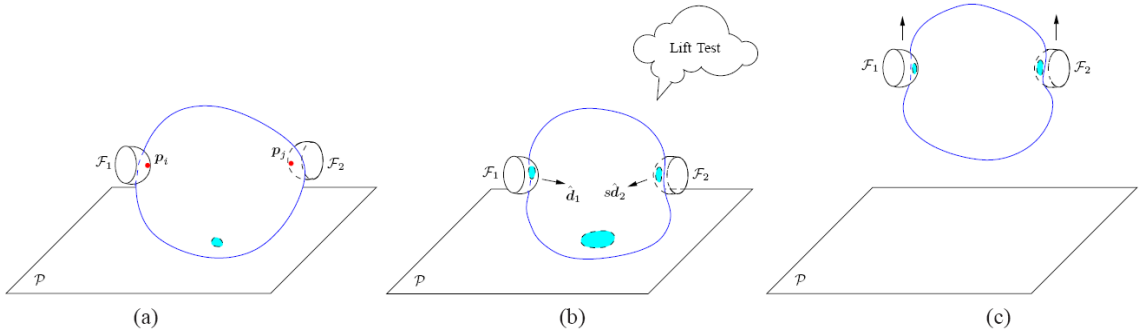

Figure 5.1 Lifting a deformable solid from the plane.

(a) resting configuration of the solid and initial finger placement; (b) squeezing (with repeated lift tests); and (c) lifting. Contact regions are shaded.

In the current phase of our work, the fingers are assumed to be translating during the squeeze in constant directions, denoted by unit vectors $\hat{\boldsymbol{d}}_1$ and $\hat{\boldsymbol{d}}_2$, respectively. Without loss of generality, let $\mathcal{F}_1$ be the moving fingertip. For every unit distance $\mathcal{F}_1$ translates in $\hat{\boldsymbol{d}}_1$, $\mathcal{F}_2$ translates in $\hat{\boldsymbol{d}}_2$ by $s \geq 0$. Thus, the squeeze action can be represented by $\rho(\hat{\boldsymbol{d}}_1, s\hat{\boldsymbol{d}}_2)$, where $\rho \geq 0$.

During the deformation the contact region with the fingertips will grow from points to areas and the contact region with the plane will also change from the original contact region due to gravity and later shrink during the lift. Denote by $\mathbb{I}$, $\mathbb{J}$, $\mathbb{K}$ the contact sets of the indices of the objects surface nodes. Their union $\mathbb{C} = \mathbb{I} \cup \mathbb{J} \cup \mathbb{K}$ consists of the indices of all contact nodes.

Algorithm 2 Two-finger pickup of a 3D solid

Input: tetrahedral mesh, table contact $\triangle \boldsymbol{p}_q\boldsymbol{p}_r\boldsymbol{p}_s$, finger contacts $\boldsymbol{p}_i$, $\boldsymbol{p}_j$, squeeze ($\hat{\boldsymbol{d}}_1$, $s\hat{\boldsymbol{d}}_2$)

1: Check if $\boldsymbol{p}_i$ and $\boldsymbol{p}_j$ form force closure with $\triangle \boldsymbol{p}_q\boldsymbol{p}_r\boldsymbol{p}_s$. If not, return failure.

2: Compute the objects resting configuration on the table from $\triangle \boldsymbol{p}_q\boldsymbol{p}_r\boldsymbol{p}_s$.

3: Squeeze the object by translating $\mathcal{F}_1$ and $\mathcal{F}_2$.

4: During the squeeze, test if the object can be lifted.

5: If so, stop squeezing and lift the object. Return success.

6: If enough squeeze has been applied and the object still cannot be picked up, report failure. Otherwise, go back to step 3.

Algorithm 2 describes how to pick up the object. Step 1 applies the procedure from (43) to check if $\boldsymbol{p}_i$, $\boldsymbol{p}_j$, and the center of $\triangle \boldsymbol{p}_q\boldsymbol{p}_r\boldsymbol{p}_s$ would be force closure on a rigid body with the same shape of the resting object. If force closure is not formed, the object will not be fully constrained and the algorithm returns failure.

Below we will first describe step 2 on modeling of the object's resting configuration when it is in contact with $\mathcal{P}$ only, then step 3 and step 5 on squeezing and lifting the object when it has active contacts with all of $\mathcal{F}_1$, $\mathcal{F}_2$, and $\mathcal{P}$, and finally step 4 on testing whether the object can be lifted after some squeeze by considering its contacts with $\mathcal{F}_1$ and $\mathcal{F}_2$ only.

5.4.1 Initial resting configuration

Before grasping the object, we need to estimate its resting configuration under gravity. Over $\triangle \boldsymbol{p}_q\boldsymbol{p}_r\boldsymbol{p}_s$, the object deforms under gravity. Since the mass center is above the triangle, force equilibrium is maintained during the deformation, which implies conservation of angular momentum and thus torque equilibrium.

We describe an iterative procedure that computes the initial resting configuration. At the beginning of each iteration, a node $\boldsymbol{p}_k, 1 \leq k \leq n$, has been displaced to the

location $\tilde{\boldsymbol{p}}_k$ and receives contact force $\boldsymbol{f}_k$ from the plane. Let the set $\mathbb{P}$ collect the indices of sliding nodes. The following steps are carried out in each iteration.

1: $\mathbb{P} \leftarrow \emptyset$.
2: Evaluates the change $\boldsymbol{\Delta}'$ from the displacement vector $\boldsymbol{\Delta}$ and the change $\bar{\boldsymbol{F}}'$ from the contact force vector $\bar{\boldsymbol{F}}$.
3: $\boldsymbol{\Delta} \leftarrow \boldsymbol{\Delta} + \boldsymbol{\Delta}'$ and $\bar{\boldsymbol{F}} \leftarrow \bar{\boldsymbol{F}} + \bar{\boldsymbol{F}}'$.
4: If no new contact node is found and, for every $k \in \mathbb{K}$, $\boldsymbol{f}_k$ is inside the friction cone at $\tilde{\boldsymbol{p}}_k$, terminate the algorithm.
5: Otherwise, handle new contact if any.
6: Identify sliding nodes and add their indices to $\mathbb{P}$.
7: Recompute the displacements of all sliding nodes.

In step 2, we fix every contact node $\boldsymbol{p}_k$ at $\tilde{\boldsymbol{p}}_k$, $k \in \mathbb{K}$. Evaluate $\boldsymbol{\Delta}'$ and $\bar{\boldsymbol{F}}'$ according to 5.6 and 5.10 after substitutions of $\boldsymbol{\Delta}'$, $\boldsymbol{F}'$, $\bar{\boldsymbol{\Delta}}'$ for $\boldsymbol{\Delta}$, $\boldsymbol{F}$, $\bar{\boldsymbol{\Delta}}$ respectively. Update $\boldsymbol{\Delta}$ and $\bar{\boldsymbol{F}}$ as described in step 3.

In step 4, a new contact exists if some node on the object would be displaced below the plane. Among all such nodes, let $\boldsymbol{p}_t$ be the one that minimizes $\tilde{\boldsymbol{p}}_t \cdot \hat{\boldsymbol{z}}$, where $\hat{\boldsymbol{z}} = (0, 0, 1)^T$. In other words, $\boldsymbol{p}_t$ would be the furthermost below $\mathcal{P}$ if it is penetrable. Step 5 adds $\boldsymbol{p}_t$ as the new contact and scale down $\boldsymbol{\delta}'_t$ such that $\tilde{\boldsymbol{p}}_t + \boldsymbol{\delta}'_t$ lies in $\mathcal{P}$.

Step 6 determines if any existing contact $\boldsymbol{p}_k$, $k \in \mathbb{K}$, is sliding by checking if $\boldsymbol{f}_k$ is outside the friction cone, or equivalently, if $(1 + \mu_{\mathcal{P}}^2)(\boldsymbol{f}_k \cdot \hat{\boldsymbol{z}})^2 < \|\boldsymbol{f}_k\|^2$, where $\mu_{\mathcal{P}}$ is the coefficient of friction between the object and the table. If the condition holds, add k to $\mathcal{P}$.

Step 7 evaluates $\bar{\boldsymbol{\Delta}}'$ and $\bar{\boldsymbol{F}}'$ again after the same substitutions in step 2, but this time we need to evaluate the extra displacements of sliding nodes. Figure 5.2 shows the situation where the contact force $\boldsymbol{f}_k$ is out of the friction cone. Project the force onto $\mathcal{P}$ to obtain $\boldsymbol{f}_{k\perp} = \boldsymbol{f} - (\boldsymbol{f} \cdot \hat{\boldsymbol{z}})\hat{\boldsymbol{z}}$. The sliding direction, represented by the polar angle α_k, is opposite to $\boldsymbol{f}_{k\perp}$ and hence known. Let $d_k \geq 0$ be the sliding distance, then the extra displacement is

$$\boldsymbol{\delta}'_k = d_k(\cos\alpha_k, \sin\alpha_k, 0)^T.$$

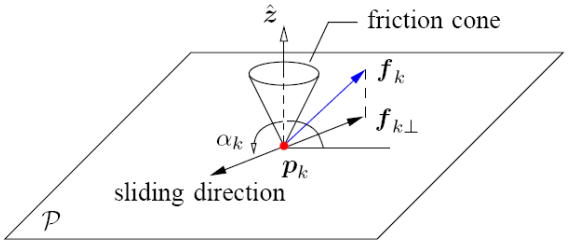

Figure 5.2 Sliding of a node on the plane.

Each $\boldsymbol{f}_k$, $k \in \mathbb{P}$ is a linear function of d_l for all $l \in \mathbb{P}$. That $\boldsymbol{f}_k$ is on the boundary of the friction cone yields a system of quadratic equations:

$$(1+\mu_{\mathcal{P}}^2)(\boldsymbol{f}_k \cdot \hat{\boldsymbol{z}})^2 = \boldsymbol{f}_k \cdot \boldsymbol{f}_k, \qquad \text{for } k \in \mathbb{P}. \tag{5.11}$$

There are $|\mathbb{P}|$ equations in $|\mathbb{P}|$ variables d_k, $k \in \mathbb{P}$. We solve the system using the homotopy continuation method (44). With the solution we can update $\boldsymbol{\Delta}$ and $\boldsymbol{F}$ and move on to the next iteration.

5.4.2 Squeezing and lifting the object

In step 3 of Algorithm 2, the object is being squeezed by $\mathcal{F}_1$ and $\mathcal{F}_2$ under translations $\rho\hat{\boldsymbol{d}}_1$ and $s\rho\hat{\boldsymbol{d}}_2$, respectively, with ρ increasing. The contact index sets $\mathbb{I}$, $\mathbb{J}$, $\mathbb{K}$ are usually growing as the squeeze depth ρ increases. The squeeze continues until either at some point the lift test(which will be introduced in the next section) is passed, or the amount of squeeze becomes too large that the object is deemed impossible to pick up under the initial finger placement and squeezing directions.

We here generalize the three-finger event-driven algorithm for in Section 4.3. Sequence ρ into $\rho_0 = 0 < \rho_1 < \cdots$ such that at $\rho = \rho_l$ some event happens to change the contact configuration. Within the interval $[\rho_l, \rho_l + 1)$ the changes $\boldsymbol{\Delta}'$ in the displacement vector and $\bar{\boldsymbol{F}}'$ in the contact forces are updated according to the modified 5.6 and 5.10.

The situation that $\boldsymbol{p}_k$ slides on a fingertip is illustrated in Figure 5.3. Let $\tilde{\boldsymbol{p}}_k$ be its current position before the slip, and $\boldsymbol{\delta}'_k$ the extra displacement due to the slip. Let $\hat{\boldsymbol{n}}_k$

be the normal at $\tilde{\boldsymbol{p}}_k$ pointing into the object. The contact force $\boldsymbol{f}_k$, out of the friction cone at $\tilde{\boldsymbol{p}}_k$, has a tangential component $\boldsymbol{f}_{i\perp} = \boldsymbol{f}_k - (\boldsymbol{f}_k \cdot \hat{\boldsymbol{n}}_k)\hat{\boldsymbol{n}}_k$.The node $\boldsymbol{p}_k$ will slide from its current position $\tilde{\boldsymbol{p}}_k$ in the opposite direction of $\boldsymbol{f}_{k\perp}$ and reach some point $\boldsymbol{q}_k$ on the great circle coplanar with $\boldsymbol{f}_{k\perp}$ and $\hat{\boldsymbol{n}}_k$. Namely, $\boldsymbol{\delta}'_k = \boldsymbol{q}_k - \tilde{\boldsymbol{p}}_k$. The unit normal

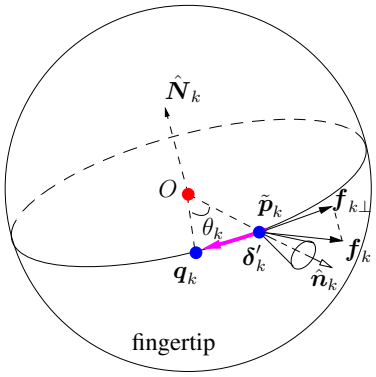

Figure 5.3 Sliding of a node on the plane.

$\hat{\boldsymbol{N}}_k$ to the plane containing this great circle is in the direction of $\hat{\boldsymbol{n}}_k \times \boldsymbol{f}_{i\perp}$. Thus, $\boldsymbol{q}_k$ is obtained from rotating $\tilde{\boldsymbol{p}}_k$ about $\hat{\boldsymbol{N}}_k$ through some angle $\theta_k < 0$. We obtain

$$\boldsymbol{q}_k = O + c_k(\tilde{\boldsymbol{p}}_k - O) + s_k(\hat{\boldsymbol{N}} \times (\tilde{\boldsymbol{p}}_k - O)), \tag{5.12}$$

where c_k and s_k are the shorthand notations for $\cos\theta_k$ and $\sin\theta_k$, respectively. Coulombs law of friction induces a quadratic equation:

$$(1 + \mu_{\mathcal{F}}^2)(\boldsymbol{f}_k \cdot \hat{\boldsymbol{n}}_k)^2 = \boldsymbol{f}_k \cdot \boldsymbol{f}_k, \tag{5.13}$$

coupled with

$$c_k^2 + s_k^2 = 1. \tag{5.14}$$

In the above, $\mu_{\mathcal{F}}$ is the coefficient of friction between the object and a fingertip.

With the updated $\boldsymbol{\delta}'_k$s, we can obtain the changes $\boldsymbol{\Delta}'$ in the displacement vector and $\bar{\boldsymbol{F}}'$ in the contact force. They depend on all d_k, $k \in \mathbb{P} \cap \mathbb{K}$, and all c_l and s_l, $l \in \mathbb{P} \cap (\mathbb{I} \cup \mathbb{J})$. We end up with a system of $2|\mathbb{P} \cap (\mathbb{I} \cup \mathbb{J})| + |\mathbb{P} \cap \mathbb{K}|$ quadratic equations in the forms

of 5.11, 5.13, or 5.14 in the same number of variables. Solve the system to update all contact slips.

We take small increments in the squeeze depth and check after each increment if any event happens. Upon such an occurrence, we can use Newton's method to polish the corresponding squeeze depth value. The contact index sets $\mathbb{I}$, $\mathbb{J}$, $\mathbb{K}$, $\mathbb{P}$ are updated whenever an event happens.

In step 5 of Algorithm 2, once the lift test is passed, the two fingers switch the action to translate upward. During the lift, the nodal contacts with the plane $\mathcal{P}$ will break one by one, and some contacts with the fingertips could also break under the gravitational force. Modeling, however, has no difference from that of squeezing. If all the contact nodes on one finger are sliding, the object slides on the finger and the pickup fails. Otherwise, the pickup succeed when the object breaks contact with the plane.

5.4.3 Lift test

When the squeeze depth is small, the friction between the object and the two fingertips is not enough to balanc the gravity if it is picked up. Starting at some squeeze depth, every time after the contact configuration is updated, a quick lift test is performed to check if the object can be picked up. This corresponds to step 4 in Algorithm 2.

The test first sets $\mathbb{C} \leftarrow \mathbb{I} \cup \mathbb{J}$, as if the supporting plane $\mathbb{P}$ were suddenly removed. The new contact displacement vector $\bar{\boldsymbol{\Delta}}$ gathers only the finger contact displacements $\boldsymbol{\delta}_k$, $k \in \mathbb{C}$, until this point. The displacement field $\boldsymbol{\Delta}$ and the contact force vector $\bar{\boldsymbol{F}}$ are recomputed according to 5.6 and 5.10. Essentially, in this computation only the displacements of the nodes in contact with the fingertips are specified, while those of the nodes in contact with the plane are not.

If $\boldsymbol{p}_k$, for some $k \in \mathbb{C}$, under its recomputed displacement penetrates into $\mathcal{F}_1$ or $\mathcal{F}_2$, then add k to $\mathbb{C}$ and reset $\boldsymbol{\delta}_k$ such that the displaced location $\tilde{\boldsymbol{p}}_k$ of $\boldsymbol{p}_k$ is on the surface of the corresponding fingertip. If some $\boldsymbol{f}_k$, $k \in \mathbb{I} \cup \mathbb{J}$, points outward from the solid, the

contact breaks at $\tilde{\boldsymbol{p}}_k$, remove k from $\mathbb{C}$. Otherwise, if $\boldsymbol{f}_k$, $k \in \mathbb{I} \cup \mathbb{J}$, stays inside the contact friction cone at $\tilde{\boldsymbol{p}}_k$, do not change $\boldsymbol{\delta}_k$.

Next, we identify the sliding nodes. Initialize $\mathbb{P} \leftarrow \emptyset$ to be the set of their indices. Consider all $k \in \mathbb{I} \cup \mathbb{J}$. If $\boldsymbol{f}_k$ points inward but outside the contact friction cone, the node $\boldsymbol{p}_k$ is regarded sliding and k is added to $\mathbb{P}$.

When the ratio $|\mathbb{P}|/|\mathbb{C}|$ is below certain threshold η, the portion of contact nodes that are predicted to be sliding is small enough. The lift test is passed. Otherwise, more squeeze is needed. And the lift test fails.

5.5 Simulation

We simulate the grasping algorithm in Section 5.4 on a sphere with radius 0.05 and mass 0.42. Its material has Young's modulus $E = 5 \times 10^4$, and Possion's ratio $\nu = 0.03$. We place the origin at the sphere's center of mass and let the xy-plane be parallel to the supporting plane $\mathcal{P}$.

Figure 5.4(a) shows a tetrahedral mesh representation of the sphere. The mesh consists of 367 vertices (with 328 on the surface), 1144 tetrahedra, and 2613 triangular faces. The triangle $\triangle \boldsymbol{p}_q \boldsymbol{p}_r \boldsymbol{p}_s$ to touch the table is colored red at the bottom. Set the frictional coefficients $\mu_{\mathcal{P}} = \mu_{\mathcal{F}} = 0.8$.

Part(b) of the figure shows the sphere resting on $\mathcal{P}$ after some deformation computed by the procedure described in Section 5.4.1. The contact region (bottom right) has grown to three triangles. Also plotted are two hemispherical fingertips $\mathcal{F}_1$ and $\mathcal{F}_2$ placed at $\boldsymbol{p}_i = (-0.00756, -0.0416, 0.0135)^T$ and $\boldsymbol{p}_j = (-0.0110, 0.0529, 0.0141)^T$, respectively.

The two fingertips then apply a squeeze specified by $(\hat{\boldsymbol{d}}_1, s\hat{\boldsymbol{d}}_2)$ with $\hat{\boldsymbol{d}}_1 = (-0.0505,$ $0.9570, -0.2856)^T$, $\hat{\boldsymbol{d}}_2 = (-0.0196, -0.9331, -0.3590)^T$, and $s = 1$. Part (c) shows the system configuration at the squeeze depth $\rho = 0.013$. The contact region (lower left) with $\mathcal{F}_1$ consists of four triangles, while the contact region (lower right) with the plane

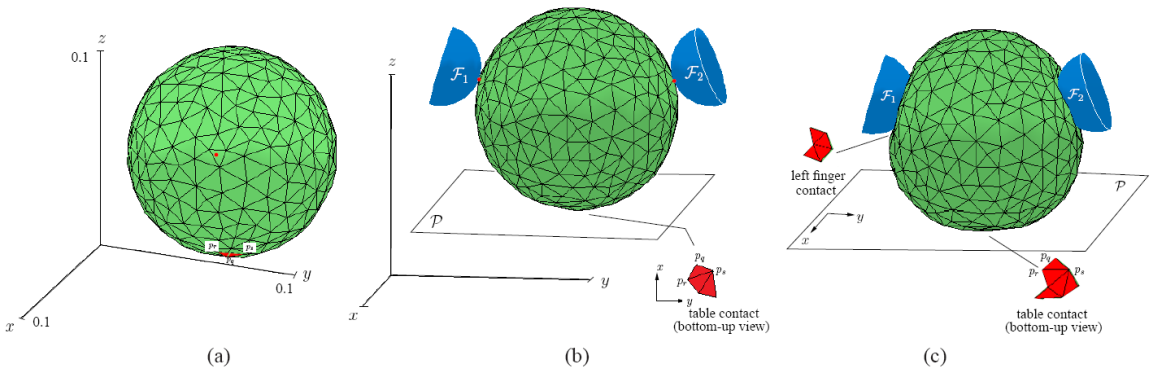

Figure 5.4 Sphere in three configurations.

(a) free; (b) resting on a horizontal plane; (c) after a squeeze by two hemispherical fingertips.

$\mathcal{P}$ consists of five.

The fingers then move straight upward to pick up the sphere. Figure 5.5 shows the configuration after the sphere breaks contact with the plane.

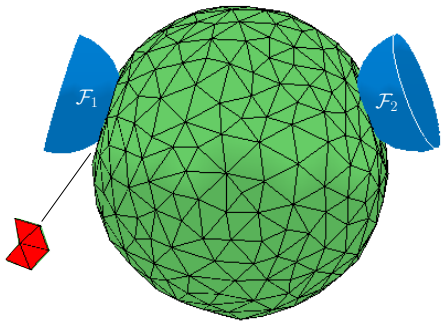

Figure 5.5 The sphere carried above the plane.

CHAPTER 6. DISCUSSION AND FUTURE WORK

In this thesis we first introduce two types of squeezes on a deformable object. A stable squeeze minimizes the potential energy for the same amount of squeeze by moving the two fingers toward each other. A pure squeeze ensures that the grasped object undergoes no rigid body motion as it deforms to eliminate unnecessary finger movements. It prevents large rotations that cannot be described under linear elasticity, on which our analysis is based.

Next we look at the best strategy to resist an adversary finger pushing against a grasped object via translation. Our introduced metric is the amount of work performed by the grasping fingers, rather than the total force they exert as frequently used in rigid body grasping. Optimal resistance strategies are first analyzed assuming fixed point and segment contacts. Then, Algorithm 1 is offered for area contacts under Coulomb friction, by incorporating the contact event detection subroutine from (3).

We also propose a simple squeeze-and-lift strategy for grasping 3D deformable objects. The idea is to model changes in shape and contact geometry during the deformation, and repeatedly conduct lift tests to predict when to switch the action from squeezing to lifting. To support the modeling, we have extended our contact-based finite element analysis to 3D, with gravity taken into account. Contact slips are handled via root finding of quadratic systems derived under Coulombs friction law and linear elasticity.

Further investigation and experimental validation need to be conducted for the introduced grasp quality measures. More understanding is needed for the stability of grasping in the presence of a disturbance, especially the grasped objects ability to absorb the dis-

turbance into its strain energy. Such absorption is expected to be more prominent with large deformations, to which the nonlinear elasticity theory needs to be applied.

The algorithm for picking up 3D deformable objects needs more extensively simulation on various objects and experimental validation using a robot hand. We would like to improve on the outcome prediction by the lift test without sacrificing its current efficiency. This is directly linked to a good accuracy in the prediction of the final finger contact regions. And also more understanding is needed about several factors that contribute to a successful pickup: global shape, geometry of contact regions, normal vs. tangential contact forces in balancing the objects weight, etc.

Comparing rigid body grasping and deformable body grasping, optimizing finger placements and squeezing directions, turning the operation into a reactive one by incorporating tactile data in the modeling for reliable slip detection/prediction are also some interesting and important future directions.

BIBLIOGRAPHY

[1] Crandall SH, Dahl NC, and Lardner TJ. *An Introduction to the Mechanics of Solids.* McGraw-Hill, Inc., 2nd edition, 1978.

[2] Gallagher RH. *Finite Element Analysis.* Prentice-Hall, Inc., 1975.

[3] Guo F, Lin H, and Jia YB. "Squeeze grasping of deformable planar objects with segment contact and stick/slip transitions," in *Proc. IEEE Int. Conf. Robot. Autom.*, 2013, pp. 3721–3726.

[4] Kerr J and Roth B. "Analysis of multifingerd hands," *Int. J. Robot. Res.*, vol. 4, pp. 3–17, 1986.

[5] Li Z. and Sastry S. S.. "Task-oriented optimal grasping by multifingered robot hands." *IEEE J. Robot. Automat.*, vol. 4, pp. 32–44, 1988.

[6] Markenscoff X and Papadimitriou CH, "Optimum grip of a polygon," *Int. J. Robot. Res.*, vol. 8, pp. 17–29, 1989.

[7] Markenscoff X, Ni L, and Papadimitriou CH. "The geometry of grasping," *International Journal of Robotics Research*, 9(1):6174, 1990.

[8] Mirtich B and Canny J, "Easily computable optimum grasps in 2-D and 3-D," in *Proc. IEEE Intl. Conf. Robot. Autom.*, 1994, pp. 739–741.

[9] Boyd SP and Wegbreit B, "Fast computation of optimal contact forces," *IEEE Trans. on Robot.*, vol. 23, pp. 1117–1132, 2007.

[10] Buss M, Faybusovich L, and Moore J, "Dikin-type algorithms for dexterous grasping force optimization," *Int. J. Robot. Res.*, vol. 17, pp. 831–839, 1998.

[11] Mishra B, "Grasp metrics: optimality and complexity," in *Algorithmic Foundations of Robotics*, K. Goldberg et al. (ed.), pp. 137–165. A. K. Peters, Boston, MA, 1995.

[12] Mishra B, Schwartz JT, and Sharir M. "On the existence and synthesis of multifinger positive grips." *Algorithmica*, 2(4):541–558, 1987.

[13] Gopalakrishnan K and Goldberg K, "D-space and deform closure grasps of deformable parts," *Int. J. Robot. Res.*, vol. 24, pp. 899–910, 2005.

[14] Nguyen VD, "Constructing force-closure grasps," *Int. J. Robot. Res.*, vol. 7, pp. 316, 1988.

[15] Bicchi A and Kumar V. "Robotic grasping and contact: a review." In *Proceedings of the IEEE International Conference on Robotics and Automation*, pp. 348–353, 2000.

[16] Rimon E and Burdick J. "On force and form closure for multiple finger grasps." In *Proceedings of the IEEE International Conference on Robotics and Automation*, pp. 1795–1800, 1996.

[17] Brost RC and Goldberg KY. "A complete algorithm for synthesizing modular fixtures for polygonal parts". In *Proceedings of the IEEE International Conference on Robotics and Automation*, pp. 535–542, 1994.

[18] van der Stappen AF,Wentink C, and Overmars MH. "Computing immobilizing grasps of polygonal parts," *International Journal of Robotics Research*, 19(5):467–479, 2000.

[19] Rimon E and Blake A. "Caging planar bodies by one-parameter two-fingered gripping systems," *International Journal of Robotics Research*, 18:299–318, 1999.

[20] Rodriguez A, Mason MT, and Ferry S. "From caging to grasping," *International Journal of Robotics Research*, 31(7):886–900, 2012.

[21] Ponce J, Sullivan S, Sudsang A, Boissonnat J, and Merlet JP. "On computing four-finger equilibrium and force-closure grasps of polyhedral objects," *International Journal of Robotics Research*, 16(1):11–35, 1997.

[22] Ponce J, Stam D, and Faverjon B. "On computing two-finger force-closure grasps of curved 2D objects," *International Journal of Robotics Research*, 12(3):263–273, 1993.

[23] Trinkle JC. "On the stability and instantaneous velocity of grasped frictionless objects," *IEEE Transactions on Robotics and Automation*, 8(5):560–572, 1992.

[24] Jia YB. "On computing optimal planar grasps," In *Proceedings of the IEEE/RSJ International Conference on Intelligent Robots and Systems*, pp. 3:427–434, 1995

[25] Wakamatsu H, Arai E, and Hirai S. "Knotting/unknotting manipulation of deformable linear objects," *International Journal of Robotics Research*, 25(4):371–395, 2006.

[26] Wakamatsu H and Hirai S. "Static modeling of linear object deformation based on differential geometry," *International Journal of Robotics Research*, 23(3):293–311, 2004.

[27] Wakamatsu H, Hirai S, and Iwata K. "Static analysis of deformable object grasping based on bounded force closure," In *Proceedings of the IEEE/RSJ International Conference on Intelligent Robots and Systems*, pp. 3324–3329, 1996.

[28] Hirai S, Tsuboi T, and Wada T. "Robust grasping manipulation of deformable objects," In *Proceedings of the IEEE International Symposium on Assembly and Task Planning*, pp. 411–416, 2001.

[29] Saha M and Isto P. "Motion planning for robotic manipulation of deformable linear objects," In *Proceedings of the IEEE International Conference on Robotics and Automation*, pp. 2478–2484, 2006.

[30] Matsuno T and Fukuda T. "Manipulation of flexible rope using topological model based on sensor information," In *Proceedings of the IEEE/RSJ International Conference on Intelligent Robots and Systems*, pp. 2638–2643, 2006.

[31] Ladd AM and Kavraki LE. "Using motion planning for knot untangling," *International Journal of Robotics Research*, 23(7):797–808, 2004.

[32] Remde A, Henrich D, and Worn H. "Picking-up deformable linear objects with industrial robots," In *Proceedings of the International Symposium on Robotics*, Tokyo, Japan, 1999.

[33] Moll M and Kavraki LE. "Path planning for deformable linear objects," *IEEE Transactions on Robotics and Automation*, 22(4):625–636, 2006.

[34] Sinha PR and Abel JM. "A contact stress model for multifingered grasps of rough objects," *IEEE Transactions on Robotics and Automation*, 8(1):7–22, 1992.

[35] Luo Q and Xiao J. "Geometric properties of contacts involving a deformable object," In *Proceedings of the IEEE Symposium on Haptic Interfaces for Virtual Environment and Teleoperator Systems*, pp. 533–538, 2006.

[36] Tian J and Jia YB. "Modeling deformations of general parametric shells grasped by a robot hand," *IEEE Transactions on Robotics*, 26(5):837–852, 2010.

[37] Francavilla A and Zienkiewicz OC. "A note on numerical computation of elastic contact problems." *International Journal for Numerical Methods in Engineering*, 9:913–924, 1975.

[38] Okamoto N and Nakazawa M. "Finite element incremental contact analysis with various frictional conditions," *International Journal for Numerical Methods in Engineering*, 14:337–357, 1979.

[39] Sachdeva TD and Ramakrishnan CV. "A finite element solution for the two-dimensional elastic contact problems with friction," *International Journal for NumericalMethods in Engineering*, 17:1257–1271, 1981.

[40] ChandraseKaran N, Haisler WE, and Goforth RE. "A finite element solution method for contact problems with friction," *International Journal for Numerical Methods in Engineering*, 24:477–495, 1987.

[41] Bower AF. *Applied Mechanics of Solids.* CRC Press, 2009.

[42] Fung YC and Tong P. *Classical and Computational Solid Mechanics*. World Scientific, 2001.

[43] Li JW, Liu H, and Cai HG. "On computing three-finger forceclosure grasps of 2-D and 3-D objects," *IEEE Trans. Robot. Automat.*, vol. 19, pp. 155–161, 2003.

[44] Allgower EL and Georg K, "Numerical path following," in *Handbook of Numerical Analysis*, vol. 5, North-Holland, 1997.